5-HT_{2C} Receptor Structures Reveal the Structural Basis of GPCR Polypharmacology

Yao Peng,[1,2,3,13] John D. McCorvy,[4,13] Kasper Harpsøe,[5,13] Katherine Lansu,[4] Shuguang Yuan,[6] Petr Popov,[7,8] Lu Qu,[1,3] Mengchen Pu,[1] Tao Che,[4] Louise F. Nikolajsen,[1,5] Xi-Ping Huang,[4,9] Yiran Wu,[1] Ling Shen,[1,10] Walden E. Bjørn-Yoshimoto,[5] Kang Ding,[1,10] Daniel Wacker,[4] Gye Won Han,[7] Jianjun Cheng,[1] Vsevolod Katritch,[7,8] Anders A. Jensen,[5] Michael A. Hanson,[11] Suwen Zhao,[1,10] David E. Gloriam,[5] Bryan L. Roth,[4,9,12,*] Raymond C. Stevens,[1,7,10,*] and Zhi-Jie Liu[1,2,3,10,14,*]

[1]iHuman Institute, ShanghaiTech University, Shanghai 201210, China

[2]Yunnan Key Laboratory of Stem Cell and Regenerative Medicine, Institute of Molecular and Clinical Medicine, Kunming Medical University, Kunming 650500, China

[3]National Laboratory of Biomacromolecules, Institute of Biophysics, Chinese Academy of Sciences, Beijing 100101, China

[4]Department of Pharmacology, University of North Carolina at Chapel Hill, Chapel Hill, NC 27599, USA

[5]Department of Drug Design and Pharmacology, University of Copenhagen, Universitetsparken 2, 2100 Copenhagen, Denmark

[6]Laboratory of Physical Chemistry of Polymers and Membranes, Ecole Polytechnique Fédérale de Lausanne (EPFL), CH B3 495 (Bâtiment CH) Station 6, Lausanne 1015, Switzerland

[7]Departments of Biological Sciences and Chemistry, Bridge Institute, Michelson Center, University of Southern California, Los Angeles, CA 90089, USA

[8]Moscow Institute of Physics and Technology, Dolgoprudny 141700, Russia

[9]National Institute of Mental Health Psychoactive Drug Screening Program (NIMH PDSP), University of North Carolina at Chapel Hill, Chapel Hill, NC 27599, USA

[10]School of Life Science and Technology, ShanghaiTech University, Shanghai 201210, China

[11]GPCR Consortium, San Marcos, CA 92078, USA

[12]Division of Chemical Biology and Medicinal Chemistry, Eshelman School of Pharmacy, University of North Carolina at Chapel Hill, Chapel Hill, NC 27599, USA

[13]These authors contributed equally

[14]Lead Contact

*Correspondence: bryan_roth@med.unc.edu (B.L.R.), stevens@shanghaitech.edu.cn (R.C.S.), liuzhj@shanghaitech.edu.cn (Z.-J.L.)

https://doi.org/10.1016/j.cell.2018.01.001

SUMMARY

Drugs frequently require interactions with multiple targets—via a process known as polypharmacology—to achieve their therapeutic actions. Currently, drugs targeting several serotonin receptors, including the 5-HT_{2C} receptor, are useful for treating obesity, drug abuse, and schizophrenia. The competing challenges of developing selective 5-HT_{2C} receptor ligands or creating drugs with a defined polypharmacological profile, especially aimed at G protein-coupled receptors (GPCRs), remain extremely difficult. Here, we solved two structures of the 5-HT_{2C} receptor in complex with the highly promiscuous agonist ergotamine and the 5-HT_{2A-C} receptor-selective inverse agonist ritanserin at resolutions of 3.0 Å and 2.7 Å, respectively. We analyzed their respective binding poses to provide mechanistic insights into their receptor recognition and opposing pharmacological actions. This study investigates the structural basis of polypharmacology at canonical GPCRs and illustrates how understanding characteristic patterns of ligand-receptor interaction and activation may ultimately facilitate drug design at multiple GPCRs.

INTRODUCTION

For effective G protein-coupled receptor (GPCR) drug discovery, some degree of receptor selectivity is essential to avoid deleterious "off-target" interactions with related GPCRs and other druggable targets (e.g., ion channels, kinases, enzymes, and so on) (Elkins et al., 2016). As GPCRs frequently have conserved orthosteric binding pockets, drugs targeting these sites often interact with multiple molecular targets; the process whereby drugs bind to many targets is known as polypharmacology.

Indeed, creating effective medications which are selective (e.g., "magic bullets") is not only difficult but also frequently unsuccessful, particularly for complex CNS disorders where the etiologies may be multifactorial and polygenic (Boyle et al., 2017). In fact, drugs with a polypharmacological basis (e.g., "magic shotguns") are frequently more effective therapeutics (Roth et al., 2004), as exemplified by the atypical antipsychotics clozapine (Clozaril) and aripiprazole (Abilify), which interact with numerous GPCRs (Jacobson et al., 2014; McCorvy and Roth, 2015; Roth et al., 2004; Shapiro et al., 2003). Additionally, carazolol and tiotropium exert their therapeutic effects by interacting with multiple adrenergic (Cherezov et al., 2007; Moukhametzianov et al., 2011) and muscarinic acetylcholine receptors (Kruse et al., 2012; Thal et al., 2016), respectively. The rational design of drugs that simultaneously interact with multiple GPCRs, therefore, has the potential to yield medications

with improved efficacy for complex disorders (Besnard et al., 2012).

Structure-based drug design approaches have facilitated the creation of selective GPCR drugs (Wang et al., 2017) with improved therapeutic profiles, as exemplified by the recent discovery of μ-opioid selective G protein-biased agonists (Manglik et al., 2016). Structure-guided approaches, perforce, require high-resolution crystal structures in order to exploit ligand-binding pocket interactions at the targeted GPCR (Wacker et al., 2017a; Wang et al., 2017). However, structure-guided drug design will not typically predict a compound's off-target actions. Ultimately, structure-based polypharmacological drug design will require many high-resolution GPCR structures with various chemotypes to illuminate how polypharmacology might be achieved at multiple defined drug targets.

The 5-HT_{2C} serotonin receptor (5-HT_{2C}) is a validated target for anti-obesity medications as illustrated by the selective 5-HT_{2C} agonist lorcaserin (Belviq). The 5-HT_{2C} is also a potential therapeutic target for depression, schizophrenia, drug addiction, and other disorders (McCorvy and Roth, 2015; Palacios et al., 2017; Pogorelov et al., 2017). Creating selective 5-HT_{2C} agonists is extremely challenging, however, as off-target agonist activity at the closely related 5-HT_{2A} and 5-HT_{2B} receptors leads to lysergic acid diethylamide (LSD)-like hallucinations (Nichols, 2016) and cardiac valvulopathy (Roth, 2007), respectively. Moreover, the 5-HT_{2C} exhibits several RNA-edited isoforms, where the non-edited isoform (INI) displays high constitutive activity that can be exploited to quantify an inverse agonist's activity (Barker et al., 1994).

To date, only two serotonin receptor structures have been solved: the 5-HT_{1B} and the 5-HT_{2B}, both in complex with ergotamine (ERG) (Wacker et al., 2013, 2017b; Wang et al., 2013) and, most recently, 5-HT_{2B} in complex with LSD (Wacker et al., 2017b). ERG is a naturally occurring ergot anti-migraine drug that contains an ergoline nucleus, a common chemotype for many drugs including LSD, bromocriptine, methysergide, and lisuride. ERG, however, has a complex polypharmacological profile with serious side effects, including cardiac valvulopathy via 5-HT_{2B} serotonin receptor agonism, which limits its widespread use as an anti-migraine medication. In contrast, ritanserin (RIT) is a selective 5-HT_2 receptor inverse agonist that has been previously investigated as an adjunct for antipsychotic medications (Den Boer et al., 2000). RIT contains a 4-benzylidenepiperidine core scaffold, which is also found in the promiscuous antipsychotic clozapine. The 4-benzylidenepiperidine is a known privileged scaffold with applications for exploiting multiple GPCRs to yield a desired polypharmacological profile (Garland and Gloriam, 2011).

Here, we present the structures of the 5-HT_{2C} INI isoform in complex with both the polypharmacological agonist ERG and the selective inverse agonist RIT in order to clarify the structural features responsible for GPCR polypharmacology. To this end, we reveal the active-like state 5-HT_{2C} receptor structure with ERG and, for comparison, an inactive state with RIT. Knowledge of these crystal structures will facilitate the basis of chemotype-specific recognition, inverse agonism, and receptor activation and will enable polypharmacological drug design.

RESULTS

Overall Structure of Agonist- and Inverse-Agonist-Bound 5-HT_{2C}

The human 5-HT_{2C} was crystallized with a thermostabilized apocytochrome b_{562}RIL (BRIL) fused to the third intracellular loop (IL3) and a single C360N$^{7.45}$ thermostabilizing mutation (superscripts denote amino acid position as described by Ballesteros and Weinstein, 1995) (Figure S1). In both structures, ERG and RIT are bound in the presumed orthosteric site and also engage a potential extended binding site encompassing the extracellular portions of transmembrane (TM) helices III, V, VI, and VII as well as extracellular loop 2 (EL2) (Figure 1A). Although disordered in other solved serotonin receptor crystal structures (Liu et al., 2013; Wacker et al., 2013, 2017b; Wang et al., 2013), all extracellular loops are well resolved in both 5-HT_{2C} crystal structures. Superposition of the ERG and RIT complexes shows shifts of 7.0 Å, 3.9 Å, and 6.6 Å at the intracellular ends of helices VI, V, and III, respectively, indicating that they represent different conformational states of the receptor (Figure 1B).

Compared to the active and inactive state structures of β_2-adrenergic receptor (β_2AR) (Rasmussen et al., 2011; Wacker et al., 2010), 5-HT_{2C}-RIT resembles the inactive state conformation of β_2AR, whereas 5-HT_{2C}-ERG shows all "active-like features" exemplified by the active state of β_2AR (Figure S2). Superposition of the 5-$HT_{1B,\ 2B,\ 2C}$-ERG and 5-HT_{2C}-RIT (Wacker et al., 2013; Wang et al., 2013) structures shows an increased opening on the intracellular ends of helices V and VI in the order 5-HT_{2B}-ERG < 5-HT_{1B}-ERG < 5-HT_{2C}-ERG compared to 5-HT_{2C}-RIT (Figures 1C and S2).

Different Binding Modes of ERG and RIT

ERG and RIT have different chemical scaffolds with distinct 5-HT_{2C} activity: ERG acts as an agonist, whereas RIT is an inverse agonist for both $G_{\alpha q}$-inositol phosphate accumulation and β-arrestin2 recruitment (Figure S3). These differential efficacies are mirrored by their distinctive binding modes as observed in the 5-HT_{2C} crystal structures, where the only common interaction is the salt bridge between the protonated nitrogen of the ligand and the conserved aspartate, D134$^{3.32}$—a canonical interaction for aminergic and many other GPCRs (Figure 2A). Compared to the ERG-bound structure, RIT binds approximately one helical turn deeper into the TM bundle (Figure 2B), which is outside of the recognized orthosteric site of other solved aminergic GPCR structures (Venkatakrishnan et al., 2013). By contrast, ERG's shallower binding pose allows an aromatic interaction only with F328$^{6.52}$ and van der Waals (vdW) contact with W324$^{6.48}$ (Figures 2B and 2H).

The deep binding pose of RIT in the 5-HT_{2C} is characterized by one of the 4-fluorophenyl groups encased in a hydrophobic pocket between helices V and VI, where it interacts via halogen-aromatic interactions with F223$^{5.47}$ and F320$^{6.44}$ and aromatic edge-to-face π-π stacking interactions with residues F328$^{6.52}$ and W324$^{6.48}$, the purported "toggle switch" important for GPCR activation (Figures 2B and 2G) (Preininger et al., 2013). We validated RIT's binding pose by mutating W324$^{6.48}$, F223$^{5.47}$ and F320$^{6.44}$, all of which decreased RIT's affinity (Figures 2E and 2F; Table S2). The W324L$^{6.48}$ mutation especially reduced

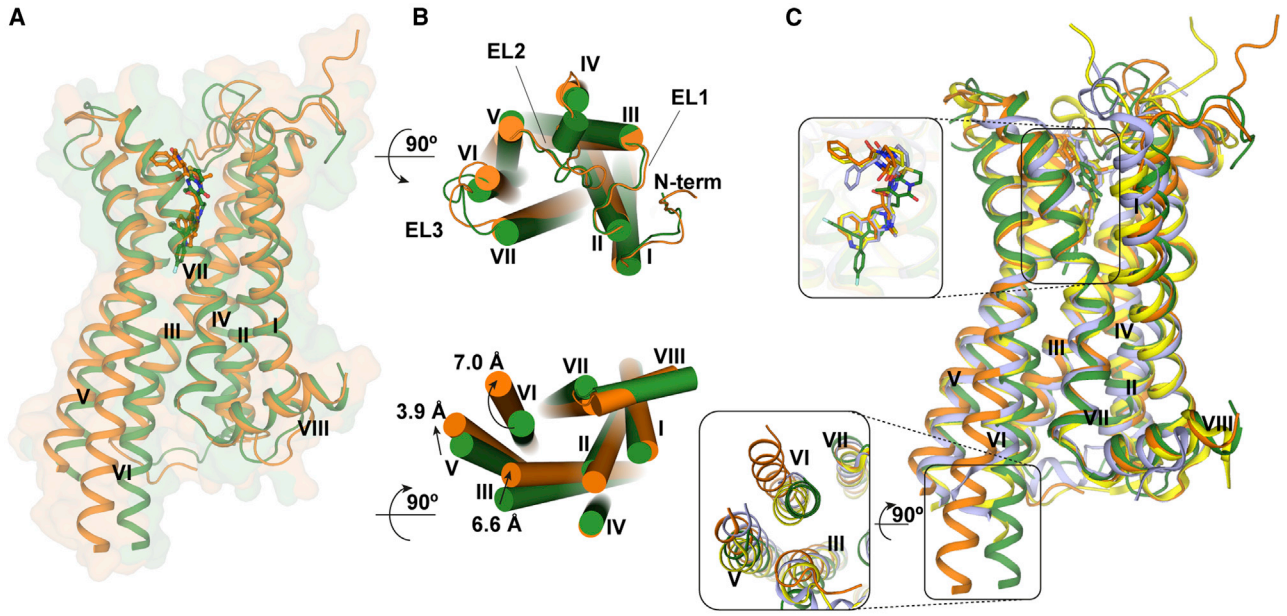

Figure 1. Overall Architecture of 5-HT$_{2C}$-ERG and -RIT and Their Comparison with 5-HT$_{1B,2B}$-ERG

(A) ERG- (agonist) and RIT- (inverse agonist) bound 5-HT$_{2C}$ are shown as orange and green cartoons. ERG and RIT are shown as orange and green balls and sticks, respectively. The helices are indicted with I through VIII.

(B) The top panel is the extracellular view. The bottom panel is the intracellular view (loops are omitted for clarity). The arrows show helical shifts as indicated (distance measured by the C$_\alpha$ atoms of I303$^{6.27}$, A245$^{5.69}$, and R157$^{3.55}$) between the 5-HT$_{2C}$-ERG and 5-HT$_{2C}$-RIT structures.

(C) Superposition of the following structures: 5-HT$_{2C}$-ERG (orange), 5-HT$_{2C}$-RIT (green), 5-HT$_{1B}$-ERG (light blue; PDB: 4IAR), and 5-HT$_{2B}$-ERG (yellow; PDB: 4IB4).

See also Figures S1 and S2 and Table S1.

RIT affinity by >1,000-fold, whereas W324F$^{6.48}$ and W324Y$^{6.48}$ mutations, which preserve the aromatic character of this residue, had substantially less effects on RIT binding affinity (Figure 2E; Table S2). These mutations support the hypothesis that the 4-fluorophenyl moiety is dependent on π-π stacking interactions below the commonly recognized aminergic orthosteric site and that these interactions with W324$^{6.48}$ are apparently driving RIT's deep binding pose.

The second 4-fluorophenyl group of RIT occupies essentially the same site as the indole of ERG and is lined by V135$^{3.33}$, T139$^{3.37}$, V185$^{4.56}$, S219$^{5.43}$, A222$^{5.46}$, and F327$^{6.51}$ (Figure 2D), with the aromatic ring systems positioned orthogonally to one another in the binding pocket (Figures 2A and 2D). The second 4-fluorophenyl group also apparently "pushes" against the backbone of helix V at residue G218$^{5.42}$ (Figure 2D). Mutation of this residue to G218A$^{5.42}$ attenuates RITs binding affinity more than 10-fold (Figure 2F) but only has a modest effect on ERG affinity, further supporting the differential binding poses (Table S2).

The thiazolopyrimidine of RIT, which stems from the charged nitrogen of the 4-benzylidenepiperidine core scaffold, is located orthogonally to the ergoline ring in the 5-HT$_{2C}$-ERG structure and is positioned toward helices II and VII interacting with Y118^{EL1}, V208^{EL2}, F327$^{6.51}$, N351$^{7.36}$ and V354$^{7.39}$ (Figure 2C). The ligand contacts at EL2 also differ between the 5-HT$_{2C}$-RIT and 5-HT$_{2C}$-ERG structures as RIT has only hydrophobic vdW contacts, but ERG engages in a hydrogen bond with the backbone of L209^{EL2} (Figure 2C). Finally, ERG's terminal benzyl moiety extends much further toward the extracellular loops of the receptor than RIT making vdW contacts with residues L209 in EL2 and V215$^{5.39}$, S334$^{6.58}$, and V335$^{6.59}$ at the topmost turns of helices V and VI (Figure 2H).

Conformational Changes between Agonist- and Inverse Agonist-Bound 5-HT$_{2C}$

Comparison of the 5-HT$_{2C}$-ERG and 5-HT$_{2C}$-RIT crystal structures also provides key insights into activation-related conformational changes in 5-HT$_{2C}$. Importantly, the intracellular end of the helix VI in 5-HT$_{2C}$-ERG is tilted outward by 7.0 Å and helix III is shifted inward by 6.6 Å compared to the 5-HT$_{2C}$-RIT structure (Figure 1B, bottom panel). Hydrogen bonds between the highly conserved D134$^{3.32}$ and Y358$^{7.43}$ are observed in both structures (Figure 3A). A comparison of the structures reveals an overall 1–2 Å binding pocket compaction with inward shift of helices V, VI, and VII around the ergoline moiety of ERG (Figure 1B, top panel). Such compaction of the binding pocket is expected for ergolines and the endogenous agonist 5-hydroxytryptamine (5-HT) (Wang et al., 2013), both of which are less bulky than the 4-(diphenylmethylene)-piperidine core of the inverse agonist RIT. These helix movements are accompanied by rotamer switches in the conserved P$^{5.50}$-I$^{3.40}$-F$^{6.44}$ (P-I-F) motif and a shift of the W324$^{6.48}$ "toggle switch" in helix VI (Figure 3B), representative of active-state-like structures at biogenic amine and other GPCRs (Venkatakrishnan et al., 2013; Wacker et al., 2013). As mentioned above, the inverse agonist RIT binds

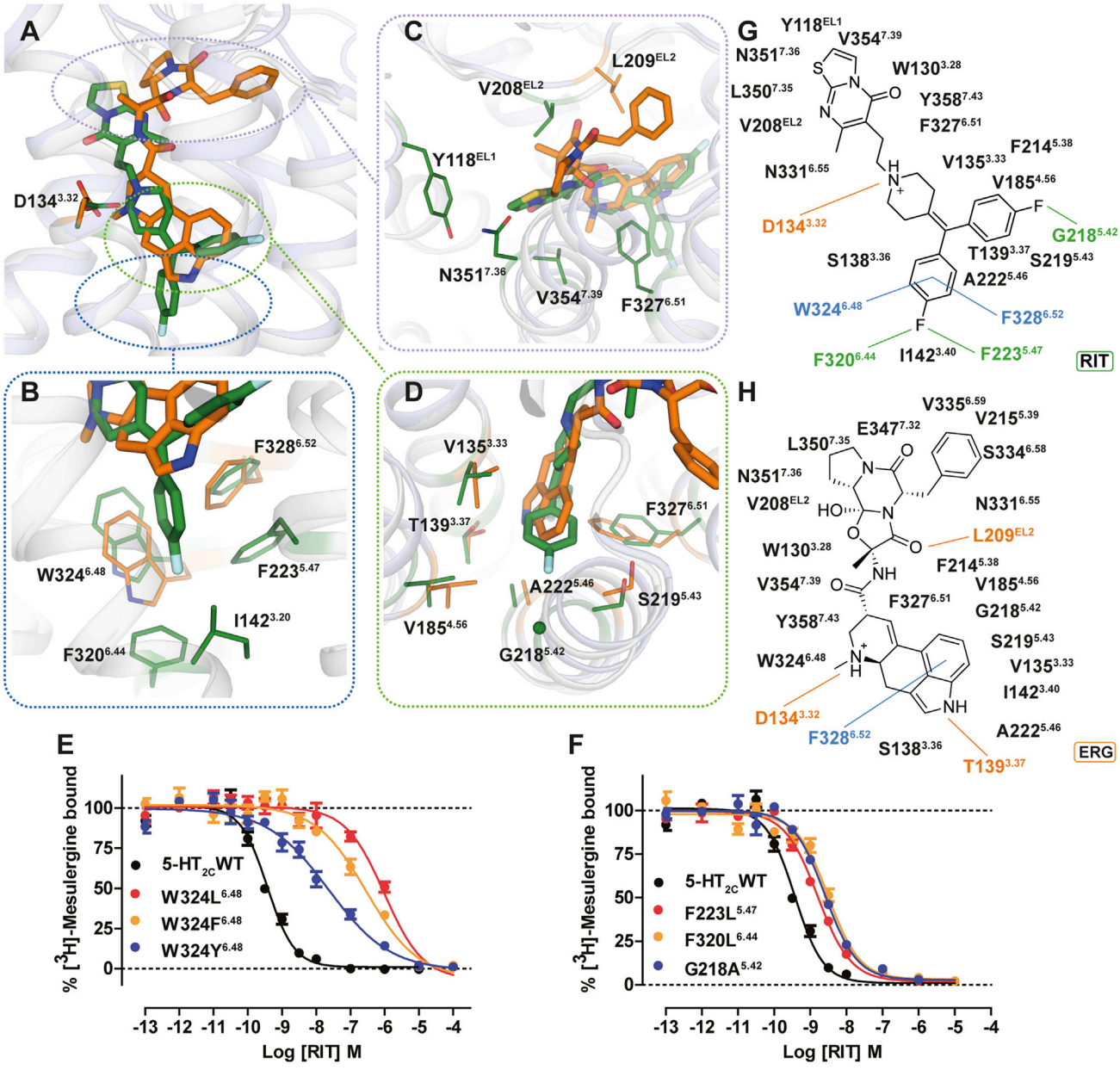

Figure 2. Different Binding Modes of ERG and RIT in 5-HT$_{2C}$

(A–D) Superposition of the 5-HT$_{2C}$-ERG (orange) and RIT (green) ligand binding pockets with an overview and close-up views of the orthosteric and extended binding sites. (A) Overall distinctive binding modes of ERG and RIT observed in 5-HT$_{2C}$. (B) The deeper binding pose of RIT and shallower binding pose of ERG. (C) Key interactions around RIT's thiazolopyrimidine as well as ERG's ergoline ring and terminal benzyl moiety. (D) The second 4-fluorophenyl group of RIT occupies the same site as the indole of ERG and positions orthogonally to each another in the binding pocket.

(E) W324$^{6.48}$ appears to be a major determinant of RIT's binding mode as measured by binding affinity loss at mutations. Binding affinity is partially recovered by the conservative mutation W324F$^{6.48}$.

(F) Mutations of residues F223$^{5.47}$, F320$^{6.44}$, and G218$^{5.42}$ also show RIT affinity loss, but less compared to W324$^{6.48}$.

(G and H) Schematic representation of RIT (G) and ERG (H) contacts with the 5-HT$_{2C}$, respectively. Lines indicate interactions types: orange, polar, salt bridges, and hydrogen bonds; blue, aromatic contacts; and green, dipolar interactions.

Data represent mean ± SEM of three independent experiments performed in duplicate (E and F).

See also Tables S2 and S7.

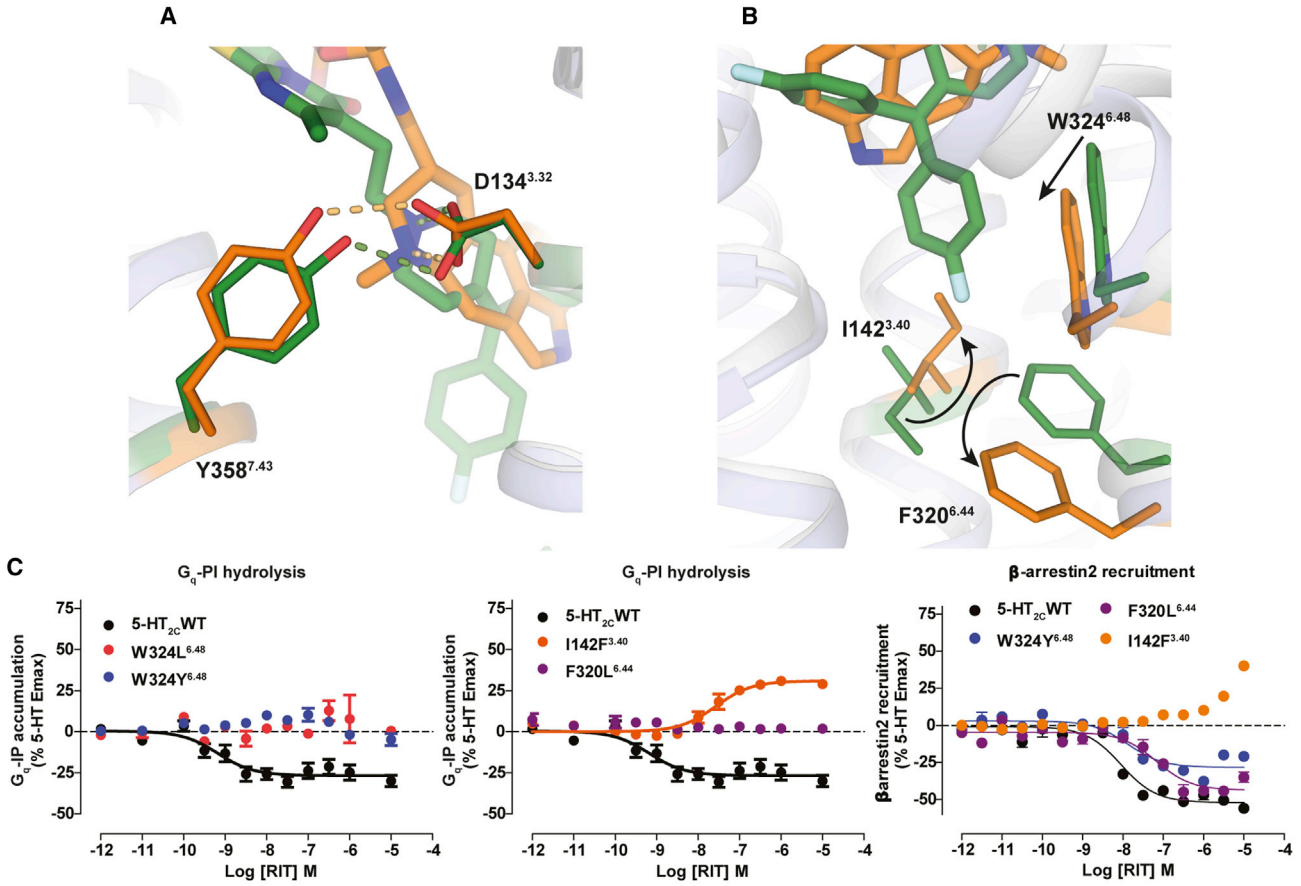

Figure 3. Conformational Changes between 5-HT$_{2C}$-ERG and -RIT Structures and Mutagenesis Validation

(A) ERG (orange sticks) and RIT (green sticks) in the binding pocket of 5-HT$_{2C}$. Key residues in 5-HT$_{2C}$-ERG and 5-HT$_{2C}$-RIT are shown in orange and green sticks, respectively. Hydrogen bonds between D134$^{3.32}$ and Y358$^{7.43}$ are shown by the dashed line.

(B) Conformational changes of I142$^{3.40}$ and F320$^{6.44}$ in the P-I-F motif and the W324$^{6.48}$ "toggle switch" in helix VI.

(C) Mutations of W324$^{6.48}$ and F320$^{6.44}$ completely abolish RIT's $G_{\alpha q}$ inverse agonism, yet retain β-arrestin2 inverse agonism. Mutations of I142$^{3.40}$ selectively abolish RIT's $G_{\alpha q}$ inverse agonism and instead show weak agonism.

Data represent mean ± SEM from three independent experiments performed in triplicate.

See also Figure S3 and Table S7.

deeper than most class A GPCR ligands in the TM helical bundle where one of its 4-fluorophenyl groups forms tight interaction with W324$^{6.48}$, I142$^{3.40}$, and F320$^{6.44}$ side chains thus apparently preventing the conformational changes in these key activation microswitches. Furthermore, the 4-fluorophenyl group of RIT is in close proximity to I142$^{3.40}$ apparently facilitating an outward shift of the intracellular end of helix III (Figure 1B, bottom panel), which potentially explains the inverse agonist activity of RIT at this receptor isoform.

To test this hypothesis, functional studies were performed with mutants of these key microswitch residues in 5-HT$_{2C}$ measuring $G_{\alpha q}$ activation and β-arrestin2 recruitment. Mutations of the "toggle switch" W324$^{6.48}$ and F320$^{6.44}$, which are part of the P-I-F trigger motif, selectively abolish RIT's $G_{\alpha q}$ inverse agonism without affecting RIT's β-arrestin2 inverse agonist activity (Figure 3C) indicating that these microswitch residues are mainly involved in the $G_{\alpha q}$ activation process. Furthermore, the I142A$^{3.40}$ mutation of the P-I-F motif also selectively abolishes RIT's $G_{\alpha q}$ inverse agonism and the I142F$^{3.40}$ mutant transforms RIT into a $G_{\alpha q}$ partial agonist with little agonist effect on arrestin recruitment (Figure 3C). This mutant I142F$^{3.40}$ likely imparts additional aromatic stacking properties to RIT, indicating that the P-I-F motif is important for RIT's inverse agonist profile (Figure 3C). These results support a model whereby the 4-fluorophenyl moiety of RIT stabilizes an inactive state of the receptor via interference with the "toggle switch" W$^{6.48}$ and "trigger motif" P$^{5.50}$-I$^{3.40}$-F$^{6.44}$ and that these microswitch residues are critical for inverse agonist activity and the $G_{\alpha q}$ activation process, in general, at the 5-HT$_{2C}$.

Multiple ERG-Serotonin Receptor Structure Complexes Reveal Determinants of Polypharmacology

To illuminate ERG's polypharmacology, we first assessed its binding affinity across the aminergic receptor family. ERG shows appreciable affinity (K_i < 10 μM) for nearly 70% of all human aminergic GPCRs with low or sub-nanomolar affinity for fifteen of

those receptors (Table S3). Further characterization of ERG activity revealed a diverse functional profile of either G protein agonist activity or β-arrestin2 recruitment activity, or in some cases both (Figure S4), indicating that ERG possesses functional selectivity across the aminergic GPCRome. However, ERG possessed no apparent G protein-dependent agonist activity at the D_3 dopamine, α_{1B}, α_{1D} or β_2 adrenergic receptors despite appreciable affinity indicating antagonism at these receptors. Interestingly, ERG was an inverse agonist at 5-HT_7 where inverse agonism has been previously reported for the structurally related ergoline analog LSD (Wacker et al., 2013). To fully illuminate ERG's polypharmacological profile, ERG was then screened at 320 non-olfactory human GPCRs via a β-arrestin2 recruitment assay (Kroeze et al., 2015), which unexpectedly revealed apparent opioid receptor agonist activity (Figure S5; Table S4).

To uncover the molecular basis for ERG's high affinity and polypharmacological profile at aminergic GPCRs, we analyzed the binding modes of ERG at the 5-$HT_{1B,\ 2B,\ 2C}$-ERG crystal structure complexes (Wacker et al., 2013; Wang et al., 2013). ERG shares a common binding mode at all three of these receptors, where the only difference is the orientation of the benzyl substituent in 5-HT_{1B}-ERG complex (Figure 1C). In regions in which ERG packs most tightly and has polar interactions—around the ergoline scaffold—all receptors demonstrating high ERG affinity exhibit highly conserved residue properties (Figures 4A and 4B, left panel). The ergoline core is surrounded by four helices where helices III and VI sandwich the planar sides of the ergoline core, whereas the other two edges are enclosed by helices V and VII. In addition to D3.32, which forms a salt bridge to most aminergic ligands, positions 3.33, 3.36, 3.37, 5.42, and 5.46 are in very close contact with ERG in all three structures and are not able to accommodate significant ERG affinity when there are significantly larger amino acids present at these residue positions. Additionally, the conserved T3.37 residue and semi-conserved A/S/T5.46 residues form either vdW interactions and/or a hydrogen bond to ERG's indole N-H. Three additional helix VI positions (6.48, 6.51, and 6.52) contribute favorable vdW and aromatic interactions where alanine or leucine mutations of these residues only lead to reduced but not abrogated ERG binding at 5-HT_{2C} (Table S2) and 5-$HT_{1B,\ 2B}$ (Wang et al., 2013). Therefore, the ergoline core is recognized by nine key residues, eight of which have specific conserved amino acid properties to enable binding. All of these properties are present in all receptors that demonstrate high ERG affinity (Figures 4A and 4B, left panel).

For ERG's cyclic tripeptide and benzyl substituents, the structures display only non-specific side-chain vdW contacts, which tolerate a high degree of flexibility and diversity of amino acids. One exception to this is the conservation of a position in EL2 (L209 in 5-HT_{2C}) of all receptors demonstrating high ERG affinity, where a small aliphatic residue such as a leucine, valine, or isoleucine is almost always present. Interestingly, the homologous EL2 residue found in 5-HT_{2B} ($L209^{EL2}$) and in 5-HT_{2A} ($L229^{EL2}$) has been recently studied as a determinant for ligand residence time, which contributes to β-arrestin recruitment (Wacker et al., 2017b). Similarly observed in the 5-HT_{2C} structure, the side chain of $L209^{EL2}$ residue points into a cavity formed by the bent tripeptide moiety of ERG and the space of the cavity is ideal for smaller aliphatic residues such as leucine, valine, or isoleucine (Figures 4A and 4B), likely contributing to ERG's shared binding pose among GPCRs.

RIT Structure Reveals Determinants of 5-HT_2 Subtype Selectivity

Although RIT is selective for 5-HT_2-family receptors, it contains a 4-benzylidenepiperidine moiety, which is a variant of a known 4-arylpiperidine GPCR privileged structure (Garland and Gloriam, 2011) (Figure 5A). The 5-HT_{2C}-RIT crystal structure reveals that D3.32, W6.48, and at least one aromatic residue at positions 5.47 and/or 6.52 are important for binding of this privileged structure. Within class A GPCRs, this sub-site is conserved in most aminergic receptors, all four opioid receptors and the melanin-concentrating hormone receptor 1 (MCR_1) (Figure 5B). Like the ergoline scaffold of ERG, the 4-benzylidenepiperidine privileged structure found in RIT ensures binding to a wide range of receptors thereby providing a molecular basis for use of this privileged structure as a starting point for polypharmacological design. Indeed, this is nicely illustrated by the polypharmacology of clozapine binding to nearly thirty aminergic receptors (Roth et al., 2004; Yadav et al., 2011a) and by cinnarizine binding to fifteen different aminergic receptors and the μ-opioid receptor (Figure 5C). By contrast, RIT binds almost exclusively to 5-HT_2 receptors with >100-fold preference over any other tested GPCR with the exception of the H_2 histamine receptor (~19-fold) (Figure 6A; Table S3).

To uncover the molecular basis for RIT's 5-HT_2 receptor selectivity, despite containing the embedded promiscuous 4-benzylidenepiperidine privileged structure, we identified residues responsible for RIT's selectivity and designed a series of mutations. We exchanged the differing binding site residues in 5-HT_{2C} with those of 5-HT_{1A} that demonstrated low affinity for RIT (Figure 6A). The most pronounced effects occurred for the two mutants $G218S^{5.42}$ (60-fold) and $V354N^{7.39}$ (425-fold), both of which are unique to 5-$HT_{2A\text{-}C}$ subtypes (Figure 6B; Table S5). In accordance with the structure showing only non-specific interactions, the other mutations, e.g., $S138C^{3.36}$, showed small or negligible effect on RIT affinity. As previously mentioned, $G218^{5.42}$ and $V354^{7.39}$ engage the second 4-fluorophenyl of RIT and the thiazolopyrimidine, both of which are structural modifications stemming from the 4-benzylidenepiperidine core scaffold that are unique to RIT (Figure 6C). Furthermore, the importance for residues 5.42 and 7.39 conferring 5-HT_2 selectivity is supported by the fact that 5-HT_{1A}, which contains S5.42 and N7.39 at these positions, has a ~1,300-fold lower affinity for RIT than does 5-HT_{2C} but sub-nanomolar affinity for ERG (Table S3). In fact, 5-HT_4, which does not demonstrate any appreciable RIT affinity at all, contains larger residues at both 5.42 and 7.39 positions (Cys and Leu, respectively). To confirm the notion that residues 5.42 and 7.39 are more important for driving RIT subtype selectivity rather than ligand promiscuity, we also sought to test clozapine at these mutations, which also contains an embedded 4-benzylidenepiperidine privileged structure. Interestingly, clozapine is only modestly affected (4-fold or below) by any of the tested binding site mutants (Table S5). These results clarify that RIT's 4-fluorophenyl and thiazolopyrimidine interactions with respective residues

A

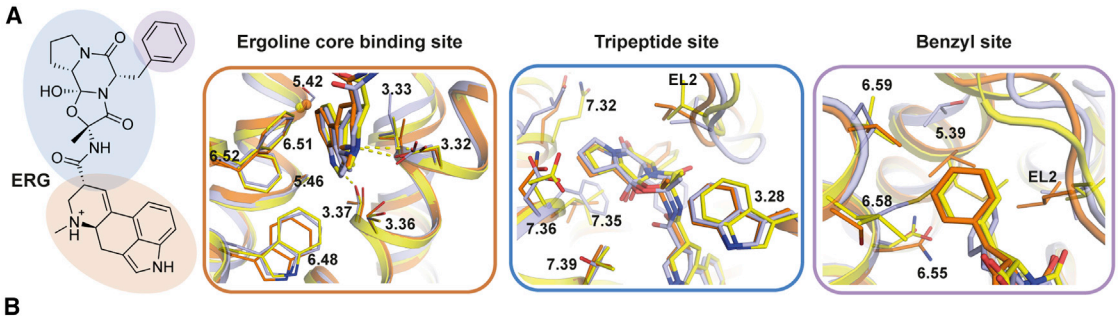

B

GPCR	Ki(nM)	3.32	3.33	3.36	3.37	5.42	5.46	6.48	6.51	6.52	3.28	EL2	7.32	7.35	7.36	7.39	EL2	5.39	6.55	6.58	6.59
5-HT$_{1D}$	0.15	D	I	C	T	S	A	W	F	F	W	L	P	F	D	T	V	T	S	L	P
5-HT$_{1B}$	0.17	D	I	C	T	S	A	W	F	F	W	V	L	F	D	T	V	T	S	M	P
α$_{2A}$	0.28	D	V	C	T	S	S	W	F	F	Y	E	R	F	K	F	I	V	Y	T	A
5-HT$_{2B}$	0.29	D	V	S	T	G	A	W	F	F	W	V	Q	L	E	V	L	M	N	L	V
5-HT$_{1A}$	0.45	D	V	C	T	S	A	W	F	F	F	T	T	G	A	N	I	T	A	L	P
5-HT$_{2A}$	0.70	D	V	S	T	G	S	W	F	F	W	L	G	L	N	V	L	V	N	A	V
5-HT$_{6}$	1.14	D	V	C	S	A	T	W	F	F	W	R	P	F	D	T	L	V	N	Q	A
D$_4$	1.17	D	V	C	T	S	S	W	F	F	L	R	P	V	S	T	L	V	H	Q	A
α$_{2C}$	1.23	D	V	C	T	S	S	W	F	F	Y	G	G	F	K	F	L	I	Y	Y	G
5-HT$_{5}$	1.63	D	V	C	T	S	A	W	F	F	W	Q	A	K	S	L	V	A	E	S	P
5-HT$_{2C}$	1.65	D	V	S	T	G	A	W	F	F	W	V	E	L	N	V	L	V	N	S	V
5-HT$_{7}$	2.46	D	V	C	T	S	A	W	F	F	F	L	L	E	R	L	I	T	S	R	P
α$_{2B}$	2.94	D	V	C	T	S	S	W	F	F	Y	K	H	F	Q	F	L	I	Y	G	A
D$_3$	3.22	D	V	C	T	S	S	W	F	F	F	S	P	Y	S	T	I	V	H	N	T
D$_2$	3.50	D	V	C	T	S	S	W	F	F	F	I	P	Y	S	T	I	V	H	N	I
α$_{1A}$	10.21	D	V	C	T	S	S	W	F	F	W	Q	E	F	K	F	I	V	M	G	S
α$_{1D}$	27.85	D	V	C	T	S	S	W	F	F	W	G	E	F	K	F	I	A	L	G	S
α$_{1B}$	29.72	D	V	C	T	S	S	W	F	F	W	G	D	F	K	F	V	A	L	G	S
β$_2$	91.23	D	V	V	T	S	S	W	F	F	W	D	K	Y	I	N	F	A	N	H	V
H$_2$	271	D	V	C	T	D	T	W	Y	F	Y	K	E	E	A	L	V	G	F	R	G
5-HT$_4$	354	D	V	T	T	C	A	W	F	F	R	V	G	W	T	L	F	A	N	D	P
5-HT$_{1e}$	507.5	D	M	C	T	S	A	W	F	F	W	T	S	A	D	T	I	T	E	V	G
D$_5$	2824	D	I	S	T	S	S	W	F	F	W	D	E	F	D	V	S	A	N	V	P
M$_4$	5660	D	Y	S	N	T	A	W	Y	N	W	F	D	W	S	Y	I	T	V	N	T
D$_1$	>10,000	D	I	S	T	S	S	W	F	F	W	D	S	F	D	V	S	A	N	L	P
β$_1$	>10,000	D	V	V	T	S	S	W	F	F	W	D	D	F	V	N	F	A	N	K	A
β$_3$	>10,000	D	V	V	T	S	S	W	F	F	W	A	G	F	L	N	F	V	N	R	A
H$_1$	>10,000	D	Y	S	T	T	N	W	Y	F	W	E	E	H	M	I	T	K	F	I	A
H$_3$	>10,000	D	Y	C	T	A	E	W	Y	T	W	Y	D	Y	E	F	A	L	M	R	A
H$_4$	>10,000	D	Y	C	T	T	E	W	Y	S	W	E	S	Y	R	F	P	L	T	L	S
M$_1$	>10,000	D	Y	S	N	T	A	W	Y	N	W	Y	E	W	E	Y	I	T	V	S	T
M$_2$	>10,000	D	Y	S	N	T	A	W	Y	N	W	Y	N	W	T	Y	I	T	V	N	T
M$_3$	>10,000	D	Y	S	N	T	A	W	Y	N	W	F	K	W	N	Y	I	T	V	N	T
M$_5$	>10,000	D	Y	S	N	T	A	W	Y	N	W	Q	V	W	H	Y	I	T	V	S	T
δ	3207	D	Y	M	F	V	A	W	I	H	V	M	V	L	H	I	L	K	V	W	T
κ	>10,000	D	Y	M	F	V	A	W	I	H	V	S	L	Y	Y	I	L	K	I	E	A
μ	>10,000	D	Y	M	F	V	A	W	I	H	V	T	T	W	H	I	L	K	V	K	A
Conserved as:		SN	IH	SU	VSP	SU	VSP		HF	HF							HA				

Figure 4. Polypharmacological Profile of ERG

(A) The chemical structure of ERG highlighting the ergoline core (brown), tripeptide (blue), and benzyl portions (purple) in the structures of 5-HT$_{2C}$ (orange), 5-HT$_{1B}$ (light blue; PDB: 4IAR), and 5-HT$_{2B}$ (yellow; PDB: 4IB4). ERG is shown as thick sticks, and the protein backbone is represented as a cartoon and the side chains of relevant amino acids as thin sticks. For clarity, the C$_\alpha$-carbon of G5.42 is depicted as a small sphere.

(B) Mean values of ERG affinities (K$_i$) in nanomolars from radioligand competition binding assays represent the mean from experiments performed in duplicate (see also Table S3). Sequence alignments of the three subsites: gray background, conservation of positions and residue types critical for ERG binding; SN, short and negative; IH, intermediate length and hydrophobic; SU, small and unbranched; VSP, very small or small and polar; HF, hydrophobic with a maximum size of Phe; HA, hydrophobic and aliphatic. Receptors are listed in order of decreasing ERG affinity (K$_i$ color scale green over white to orange) but separated into aminergic and non-aminergic receptors.

See also Figures S4 and S5 and Tables S3 and S4.

G218$^{5.42}$ and V354$^{7.39}$, which are residues exclusive to 5-HT$_2$ receptors, are primary determinants of RIT's 5-HT$_2$ selectivity.

DISCUSSION

Here, we determined agonist- and antagonist-stabilized structures of the 5-HT$_{2C}$ receptor, a molecular target important for drugs that can treat diseases as diverse as obesity, schizophrenia, and drug abuse. Importantly, the 5-HT$_{2C}$-ERG and -RIT structures not only reveal the molecular determinants for selective ligand binding across GPCRs but also reveal a structural basis for promiscuous ligand ergotamine binding across several receptor subtypes (e.g., serotonin, dopamine, adrenergic, histamine, muscarinic, and opioid). We anticipate that our findings will

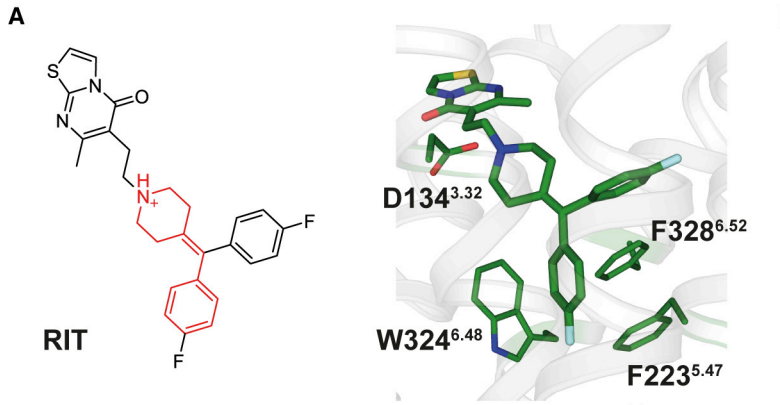

B

GPCR	3.32	6.48	5.47	6.52	#ligands
5-HT$_{1A}$	D	W	F	F	186
5-HT$_{1B}$	D	W	F	F	34
5-HT$_{1D}$	D	W	F	F	34
5-HT$_{1e}$	D	W	F	F	2
5-HT$_{2A}$	D	W	F	F	298
5-HT$_{2B}$	D	W	F	F	73
5-HT$_{2C}$	D	W	F	F	151
5-HT$_{4}$	D	W	F	F	6
5-HT$_{5}$	D	W	F	F	5
5-HT$_{6}$	D	W	F	F	16
5-HT$_{7}$	D	W	F	F	37
M$_1$	D	W	F	N	32
M$_2$	D	W	F	N	46
M$_3$	D	W	F	N	62
M$_4$	D	W	F	N	11
M$_5$	D	W	F	N	10
α$_{1A}$	D	W	F	F	20
α$_{1B}$	D	W	F	F	17
α$_{1D}$	D	W	F	F	13
α$_{2A}$	D	W	F	F	25
α$_{2B}$	D	W	F	F	10
α$_{2C}$	D	W	F	F	11
β$_1$	D	W	F	F	9
β$_2$	D	W	F	F	11
β$_3$	D	W	F	F	6
D$_1$	D	W	F	F	122
D$_2$	D	W	F	F	430
D$_3$	D	W	F	F	72
D$_4$	D	W	F	F	169
D$_5$	D	W	F	F	10
H$_1$	D	W	F	F	271
H$_2$	D	W	F	F	2
H$_3$	D	W	F	T	59
H$_4$	D	W	F	S	12
δ	D	W	F	H	189
κ	D	W	F	H	238
μ	D	W	F	H	378
NOP	D	W	F	Q	300
MCH$_1$	D	W	F	Y	11
Cons.	D	W	1AR		

C

Cinnarizine
5-HT$_{1A}$, 5-HT$_{2A}$, 5-HT$_{2B}$, D$_2$, D$_3$, H$_1$, H$_4$, M$_1$, M$_3$, M$_4$, M$_5$, α$_{1B}$, α$_{1D}$, α$_{2A}$, α$_{2C}$, μ

Clozapine
5-HT$_{1A}$, 5-HT$_{1B}$, 5-HT$_{1D}$, 5-HT$_{1e}$, 5-HT$_{1F}$, 5-HT$_{2A}$, 5-HT$_{2B}$, 5-HT$_{2C}$, 5-HT$_6$, 5-HT$_7$, D$_1$, D$_2$, D$_3$, D$_4$, D$_5$, H$_1$, H$_2$, H$_4$, M$_1$, M$_2$, M$_3$, M$_4$, M$_5$, α$_{1A}$, α$_{1B}$, α$_{2A}$, α$_{2B}$, α$_{2C}$

Cyproheptadine
5-HT$_{1A}$, 5-HT$_{2A}$, 5-HT$_{2B}$, 5-HT$_{2C}$, 5-HT$_6$, 5-HT$_7$, D$_1$, D$_2$, D$_3$, H$_1$, H$_2$, M$_1$, M$_2$, M$_3$, M$_4$, M$_5$, α$_{1A}$, α$_{1B}$, α$_{1D}$, α$_{2A}$, α$_{2B}$, α$_{2C}$

CHEMBL115280
D$_2$, D$_3$, H$_1$, κ, μ

CHEMBL330291
δ, μ, κ, NOP

CHEMBL1914849
MCH$_1$

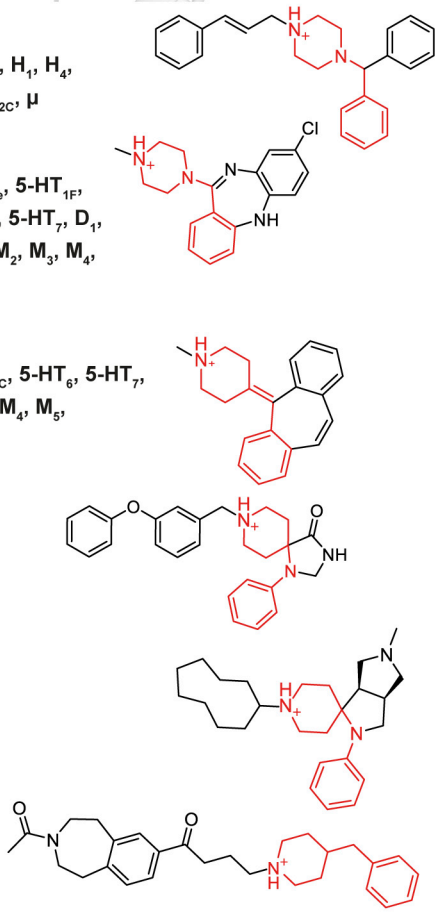

Figure 5. Polypharmacology of the 4-Benzylidenepiperidine Privileged Structure

(A) The interactions between the 4-benzylidenepiperidine of RIT and its surrounding residues in the 5-HT$_{2C}$-RIT structure.

(B) Sequence alignments of the privileged structure subsites with the number of ligands identified in a search for GPCR ligands in ChEMBL containing the privileged structure and K_i < 1 μM. Conservation of positions critical for binding is shown in a gray background, and conservation is assessed by the residue properties crucial for interaction; 1AR, aromatic residue in at least one of the two positions.

(C) Examples of ligands identified in the search with confirmed GPCR targets (K_i < 1 μM) are listed, and the privileged structure is highlighted in red in the chemical structures. For cinnarizine and clozapine, the hits from ChEMBL (Bento et al., 2014) have been supplemented with hits from the PDSP K_i database (Yadav et al., 2011a).

ultimately prove fundamental for not only the design of selective 5-HT$_{2C}$ ligands, such as lorcaserin (Belviq), which, similar to RIT, has G218$^{5.42}$ as a major selectivity determinant (Figure S6; Table S6), but also will provide a primer for understanding how drugs like clozapine interact with multiple targets, ultimately facilitating a structure-guided polypharmacological approach to drug design.

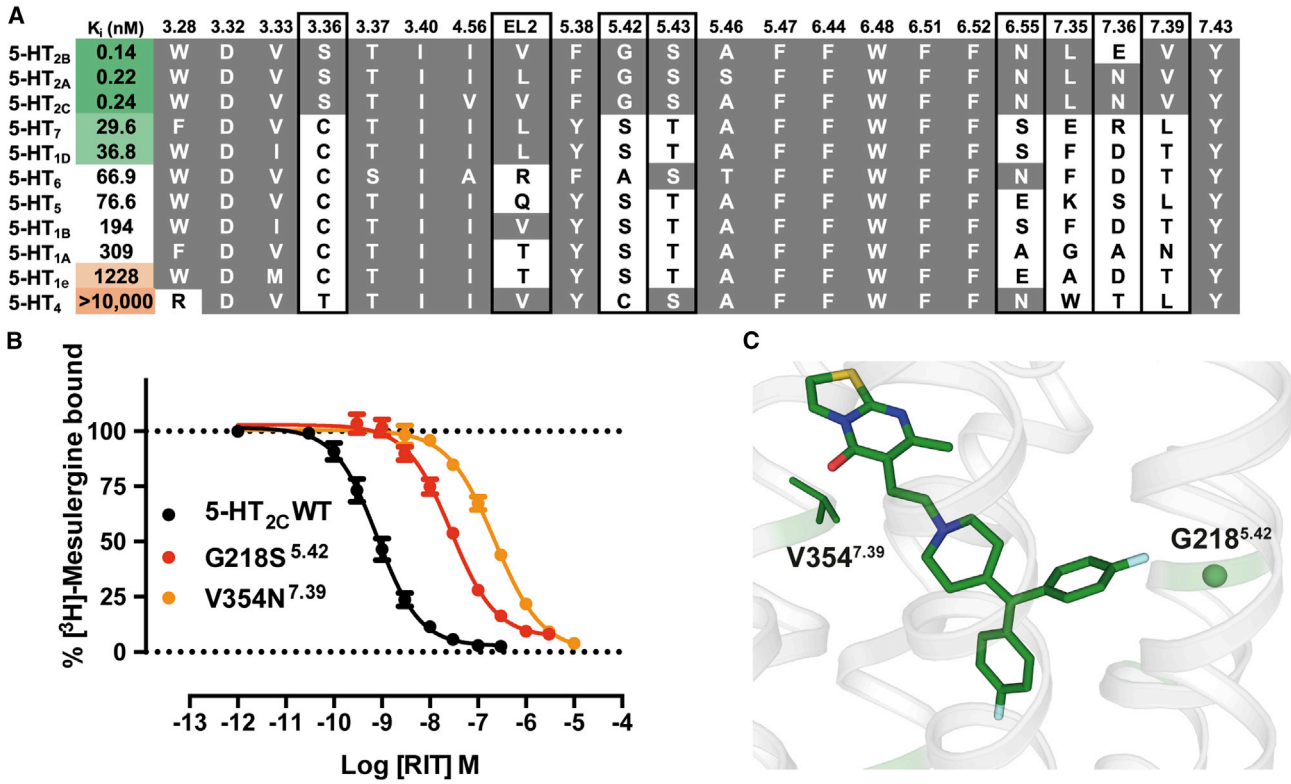

	Ki (nM)	3.28	3.32	3.33	3.36	3.37	3.40	4.56	EL2	5.38	5.42	5.43	5.46	5.47	6.44	6.48	6.51	6.52	6.55	7.35	7.36	7.39	7.43
5-HT2B	0.14	W	D	V	S	T	I	I	V	F	G	S	A	F	F	W	F	F	N	L	E	V	Y
5-HT2A	0.22	W	D	V	S	T	I	I	L	F	G	S	S	F	F	W	F	F	N	L	N	V	Y
5-HT2C	0.24	W	D	V	S	T	I	V	V	F	G	S	A	F	F	W	F	F	N	L	N	V	Y
5-HT7	29.6	F	D	V	C	T	I	I	L	Y	S	T	A	F	F	W	F	F	S	E	R	L	Y
5-HT1D	36.8	W	D	I	C	T	I	I	L	Y	S	T	A	F	F	W	F	F	S	F	D	T	Y
5-HT6	66.9	W	D	V	C	S	I	A	R	F	A	S	T	F	F	W	F	F	N	F	D	T	Y
5-HT5	76.6	W	D	V	C	T	I	I	Q	Y	S	T	A	F	F	W	F	F	E	K	S	L	Y
5-HT1B	194	W	D	I	C	T	I	I	V	Y	S	T	A	F	F	W	F	F	S	F	D	T	Y
5-HT1A	309	F	D	V	C	T	I	I	T	Y	S	T	A	F	F	W	F	F	A	G	A	N	Y
5-HT1e	1228	W	D	M	C	T	I	I	T	Y	S	T	A	F	F	W	F	F	E	A	D	T	Y
5-HT4	>10,000	R	D	V	T	T	I	I	V	Y	C	S	A	F	F	W	F	F	N	W	T	L	Y

Figure 6. Ritanserin's Selectivity on 5-HT$_2$ Receptors

(A) Mean values of RIT affinities (K_i) in nanomolars for radioligand competition binding assays from experiments performed in duplicate. Sequence alignment of the RIT binding site residues in the eleven serotonin receptors for which RIT's binding affinity was determined. Conservation of residue type by 5-HT$_{2C}$ is indicated by a gray background, and mutated positions are indicated with black boxes.

(B) The unique residue types in positions 5.42 and 7.39 of the 5-HT$_{2A\text{-}C}$ receptors (see A) appear as major determinants of the RIT selectivity for these receptor subtypes as binding affinity decreased when mutated in 5-HT$_{2C}$ to the corresponding residues of 5-HT$_{1A}$, i.e., G218S$^{5.42}$ and V354N$^{7.39}$. Data represent mean ± SEM of three independent experiments performed in duplicate.

(C) The interactions between RIT and G218$^{5.42}$ and V354$^{7.39}$ in the 5-HT$_{2C}$-RIT structure.

See also Figure S6 and Tables S3 and S5–S7.

To unveil the structural basis of GPCRs' polypharmacology, we identified ten key conserved amino-acid residues critical for ERG promiscuity by using sequence alignments of residues that interact with the ergoline core and benzyl sub-sites at eighteen aminergic receptors that show high ERG affinity (<30 nM). In fact, deviation from these conserved amino acid types reliably predicted decreased ERG affinity, dependent on position and type of amino acid present. To estimate the full target profile of ERG, we performed a sequence alignment focused on the ten ERG-interacting residues at all class A GPCRs and found that ERG's polypharmacology is not confined to aminergic GPCRs but also extends to the delta-opioid receptor (δ), which has a semi-conserved binding site and, thus, lower affinity. These ten conserved amino-acid residues can now be used to guide structure-based design of polypharmacological ligands at these receptor types, especially for computational-based methods that can predict known and unexpected drug targets (Besnard et al., 2012; Chaudhari et al., 2017). Additionally, we identify two positions for determining RIT 5-HT$_2$ selectivity, with V354$^{7.39}$ having the largest effect on selectivity (425-fold; Table S5), which should be avoided in design of compounds with polypharmacology profiles. This is nicely illustrated by examining cyproheptadine (Periactin), whose structure is based on the same 4-(diphenylmethylene)-piperidine core as RIT but lacks the thiazolopyrimidine (Figure 5C) interacting with V354$^{7.39}$. Cyproheptadine displays reduced selectivity between aminergic receptors (https://pdsp.unc.edu/databases/kidb.php) and within the 5-HT receptors, e.g., the 5-HT$_{2C}$ versus 5-HT$_{1A}$ selectivity is reduced from 1,288-fold for RIT (Table S3) to 4- to 26-fold for cyproheptadine (Toll et al., 1998). Taken together, our analysis of the 5-HT$_{2C}$-ERG and -RIT structures in comparison with the previously published 5-HT$_{1B/2B}$-ERG structures reveal highly conserved receptor sub-pockets and ligand sub-structures responsible for GPCR polypharmacology in contrast to the interactions that confer ligand selectivity.

The successful polypharmacological drugs, however, depend on a diverse range of incorporated pharmacological activity (e.g., agonism, biased agonism, inverse agonism) at each respective target. As mentioned, clozapine binds to nearly 30 aminergic receptors at which clozapine mainly demonstrates

antagonist activity (Roth et al., 2004). However, clozapine has also been shown to demonstrate functional selectivity at 5-HT_{2A} receptor (Yadav et al., 2011b) as well as inverse agonism at 5-HT_7 receptor (Thomas et al., 1998). Therefore, incorporating functional selectivity or biased agonism into a drug's polypharmacological profile can often lead to novel avenues of therapeutic potential, as observed with aripiprazole, a polypharmacological drug that demonstrates functional selectivity (Shapiro et al., 2003; Tuplin and Holahan, 2017). The 5-HT_{2C}-RIT and the ERG crystal structures shed light on such a strategy with RIT's and ERG's opposing pharmacological action leading to different activation states of the 5-HT_{2C}. We identified key areas in both the P-I-F and the W6.48 "toggle" microswitch trigger motifs that appear to be mainly involved in the 5-HT_{2C}-$G_{\alpha q}$ activation process and not necessarily involved in β-arrestin recruitment, which may serve as a starting point for pathway-selective drugs. In addition, we also show that RIT interferes with these microswitch motifs to produce $G_{\alpha q}$-dependent inverse agonism, which appears to be an important mechanism for stabilizing the inactive state of the receptor. Targeting these motifs may represent a potential mechanism for the design of novel inverse agonists, especially aimed at 5-HT_2 receptors where current inverse agonists aimed at this receptor subtype (e.g., pimavanserin) are indicated for schizophrenia and psychosis-associated with Parkinson's disease (Meltzer and Roth, 2013).

It is worth noting that the non-edited INI isoform of the 5-HT_{2C} was selected to study the ligand-receptor interactions and its indications to GPCR polypharmacology. There are signaling differences among isoforms, and studying other 5-HT_{2C} isoforms could result in different pharmacological profiles for the specific receptor subtype. However, because the binding pocket residues are identical in the edited isoforms, our inferences are not necessarily isoform specific, and we expect our conclusion concerning polypharmacology and selectivity, which are based on ligand-receptor binding, to be generally applicable.

Our knowledge of the molecular basis for polypharmacology is still in its infancy, and it remains difficult to predict what combination of targets will ultimately lead to more effective treatments of complex diseases. Evident is the fact that some of the most successful GPCR drugs (e.g., Clozaril or Abilify for schizophrenia) bind to multiple receptors and that key target combinations ultimately provide the drug's efficacy. Obtaining a better understanding of the structural basis for GPCR polypharmacology is thus the first step toward a rational utilization of this principle for future GPCR drug design. Our approach also may be broadly useful for determining the polypharmacological determinants of other privileged scaffolds or promiscuous drugs and provide a roadmap for the rational design of polypharmacological ligands.

STAR★METHODS

Detailed methods are provided in the online version of this paper and include the following:

SUPPLEMENTAL INFORMATION

Supplemental Information includes six figures and seven tables and can be found with this article online at https://doi.org/10.1016/j.cell.2018.01.001.

ACKNOWLEDGMENTS

This work was supported by grants from the Ministry of Science and Technology of China (2014CB910400 and 2015CB910104), the National Nature Science Foundation of China (31330019) (to Z.J.L.), the NIH (R01MH112205 and U19MH82441), the Michael Hooker Distinguished Professorship, the NIMH Psychoactive Drug Screening Program (271201300017C-4-01) (to B.L.R., J.M., and others from the Roth lab), the NIH (U54GM094618) (to V.K.), the Russian Science Foundation (16-14-10273) (to P.P.), and the Lundbeck Foundation (R163-2013-16327) (to D.E.G.). We thank the Shanghai Municipal Government and ShanghaiTech University for financial support. The diffraction data were collected at the BL41XU of SPring-8 (JASRI proposal 2015B1031 and 2016A2731), GM/CA at APS of Argonne National Lab, and X06SA beamline at the Swiss Light Source of the Paul Scherrer Institute. We thank K. Hasegawa, H. Okumura, H. Murakami, M. Audet, M. Wang, C. Huang, and V. Olieric for their help with data collection. We thank the Cloning, Cell Expression, Assay, and Protein Purification Core Facilities of iHuman Institute for their support. We thank I. Wilson for careful review and insightful discussions on the manuscript; A. Walker for assistance with the manuscript; and T. Hua, V. Cherezov, T. Tsonkov, G. Song, W. Shui, D. Liu, H. Tao, G. Zhong, F. Xu, B. Wu, Q. Zhao, and W. Liu for helpful discussions.

AUTHOR CONTRIBUTIONS

Conceptualization, B.L.R., R.C.S., and Z.-J.L.; Methodology, Y.P., J.D.M., and K.H.; Validation, G.W.H. and V.K.; Formal Analysis, Y.P., J.D.M., K.H., S.Y., P.P., M.P., L.Q., T.C., L.F.N., X.-P.H., Y.W., K.L., L.S., W.E.B.-Y., K.D., D.W., J.C., V.K., A.A.J., M.A.H., S.Z., D.E.G., B.L.R., R.C.S., and Z.-J.L.; Investigation, Y.P., J.D.M., and K.H.; Writing—Original Draft, Y.P., J.D.M., and K.H.; Writing—Reviewing, & Editing, Y.P., J.D.M., K.H. M.A.H., V.K., D.E.G., B.L.R., R.C.S., and Z.-J.L.; Visualization, Y.P., J.D.M., K.H. M.A.H., V.K., and D.E.G.; Supervision, B.L.R., R.C.S., and Z.-J.L.

DECLARATION OF INTERESTS

All authors declare no competing interests.

Received: July 14, 2017
Revised: October 25, 2017
Accepted: January 3, 2018
Published: February 1, 2018

REFERENCES

Abagyan, R., and Totrov, M. (1994). Biased probability Monte Carlo conformational searches and electrostatic calculations for peptides and proteins. J. Mol. Biol. *235*, 983–1002.

Adams, P.D., Afonine, P.V., Bunkóczi, G., Chen, V.B., Davis, I.W., Echols, N., Headd, J.J., Hung, L.W., Kapral, G.J., Grosse-Kunstleve, R.W., et al. (2010). PHENIX: a comprehensive Python-based system for macromolecular structure solution. Acta Crystallogr. D Biol. Crystallogr. *66*, 213–221.

Alexandrov, A.I., Mileni, M., Chien, E.Y., Hanson, M.A., and Stevens, R.C. (2008). Microscale fluorescent thermal stability assay for membrane proteins. Structure *16*, 351–359.

Ballesteros, J.A., and Weinstein, H. (1995). Integrated methods for the construction of three-dimensional models and computational probing of structure-function relations in G protein-coupled receptors. In Methods in Neurosciences, C.S. Stuart, ed. (Academic Press), pp. 366–428, [19].

Barker, E.L., Westphal, R.S., Schmidt, D., and Sanders-Bush, E. (1994). Constitutively active 5-hydroxytryptamine2C receptors reveal novel inverse agonist activity of receptor ligands. J. Biol. Chem. *269*, 11687–11690.

Barnea, G., Strapps, W., Herrada, G., Berman, Y., Ong, J., Kloss, B., Axel, R., and Lee, K.J. (2008). The genetic design of signaling cascades to record receptor activation. Proc. Natl. Acad. Sci. USA *105*, 64–69.

Bento, A.P., Gaulton, A., Hersey, A., Bellis, L.J., Chambers, J., Davies, M., Krüger, F.A., Light, Y., Mak, L., McGlinchey, S., et al. (2014). The ChEMBL bioactivity database: an update. Nucleic Acids Res. *42*, D1083–D1090.

Besnard, J., Ruda, G.F., Setola, V., Abecassis, K., Rodriguiz, R.M., Huang, X.P., Norval, S., Sassano, M.F., Shin, A.I., Webster, L.A., et al. (2012). Automated design of ligands to polypharmacological profiles. Nature *492*, 215–220.

Bourdon, D.M., Wing, M.R., Edwards, E.B., Sondek, J., and Harden, T.K. (2006). Quantification of isozyme-specific activation of phospholipase C-beta2 by Rac GTPases and phospholipase C-epsilon by Rho GTPases in an intact cell assay system. Methods Enzymol. *406*, 489–499.

Boyle, E.A., Li, Y.I., and Pritchard, J.K. (2017). An expanded view of complex traits: from polygenic to omnigenic. Cell *169*, 1177–1186.

Caffrey, M., and Cherezov, V. (2009). Crystallizing membrane proteins using lipidic mesophases. Nat. Protoc. *4*, 706–731.

Chaudhari, R., Tan, Z., Huang, B., and Zhang, S. (2017). Computational polypharmacology: a new paradigm for drug discovery. Expert Opin. Drug Discov. *12*, 279–291.

Cheng, J., McCorvy, J.D., Giguere, P.M., Zhu, H., Kenakin, T., Roth, B.L., and Kozikowski, A.P. (2016). Design and discovery of functionally selective serotonin 2C (5-HT2C) receptor agonists. J. Med. Chem. *59*, 9866–9880.

Cherezov, V., Rosenbaum, D.M., Hanson, M.A., Rasmussen, S.G., Thian, F.S., Kobilka, T.S., Choi, H.J., Kuhn, P., Weis, W.I., Kobilka, B.K., and Stevens, R.C. (2007). High-resolution crystal structure of an engineered human beta2-adrenergic G protein-coupled receptor. Science *318*, 1258–1265.

Cherezov, V., Hanson, M.A., Griffith, M.T., Hilgart, M.C., Sanishvili, R., Nagarajan, V., Stepanov, S., Fischetti, R.F., Kuhn, P., and Stevens, R.C. (2009). Rastering strategy for screening and centring of microcrystal samples of human membrane proteins with a sub-10 microm size X-ray synchrotron beam. J. R. Soc. Interface *6* (*Suppl 5*), S587–S597.

Collaborative Computational Project, Number 4 (1994). The CCP4 suite: programs for protein crystallography. Acta Crystallogr. D Biol. Crystallogr. *50*, 760–763.

Den Boer, J.A., Vahlne, J.O., Post, P., Heck, A.H., Daubenton, F., and Olbrich, R. (2000). Ritanserin as add-on medication to neuroleptic therapy for patients with chronic or subchronic schizophrenia. Hum. Psychopharmacol. *15*, 179–189.

Elkins, J.M., Fedele, V., Szklarz, M., Abdul Azeez, K.R., Salah, E., Mikolajczyk, J., Romanov, S., Sepetov, N., Huang, X.P., Roth, B.L., et al. (2016). Comprehensive characterization of the Published Kinase Inhibitor Set. Nat. Biotechnol. *34*, 95–103.

Emsley, P., Lohkamp, B., Scott, W.G., and Cowtan, K. (2010). Features and development of Coot. Acta Crystallogr. D Biol. Crystallogr. *66*, 486–501.

Garland, S.L., and Gloriam, D.E. (2011). A ligand's view of target similarity: chemogenomic binding site-directed techniques for drug discovery. Curr. Top. Med. Chem. *11*, 1872–1881.

Huang, X.P., Setola, V., Yadav, P.N., Allen, J.A., Rogan, S.C., Hanson, B.J., Revankar, C., Robers, M., Doucette, C., and Roth, B.L. (2009). Parallel functional activity profiling reveals valvulopathogens are potent 5-hydroxytryptamine(2B) receptor agonists: implications for drug safety assessment. Mol. Pharmacol. *76*, 710–722.

Isberg, V., Mordalski, S., Munk, C., Rataj, K., Harpsøe, K., Hauser, A.S., Vroling, B., Bojarski, A.J., Vriend, G., and Gloriam, D.E. (2016). GPCRdb: an information system for G protein-coupled receptors. Nucleic Acids Res. *44* (D1), D356–D364.

Jacobson, K.A., Costanzi, S., and Paoletta, S. (2014). Computational studies to predict or explain G protein coupled receptor polypharmacology. Trends Pharmacol. Sci. *35*, 658–663.

Jordan, M., Schallhorn, A., and Wurm, F.M. (1996). Transfecting mammalian cells: optimization of critical parameters affecting calcium-phosphate precipitate formation. Nucleic Acids Res. *24*, 596–601.

Kabsch, W. (2010). Xds. Acta Crystallogr. D Biol. Crystallogr. *66*, 125–132.

Kroeze, W.K., Sassano, M.F., Huang, X.P., Lansu, K., McCorvy, J.D., Giguère, P.M., Sciaky, N., and Roth, B.L. (2015). PRESTO-Tango as an open-source resource for interrogation of the druggable human GPCRome. Nat. Struct. Mol. Biol. *22*, 362–369.

Kruse, A.C., Hu, J., Pan, A.C., Arlow, D.H., Rosenbaum, D.M., Rosemond, E., Green, H.F., Liu, T., Chae, P.S., Dror, R.O., et al. (2012). Structure and dynamics of the M3 muscarinic acetylcholine receptor. Nature *482*, 552–556.

Liu, W., Wacker, D., Gati, C., Han, G.W., James, D., Wang, D., Nelson, G., Weierstall, U., Katritch, V., Barty, A., et al. (2013). Serial femtosecond crystallography of G protein-coupled receptors. Science *342*, 1521–1524.

Manglik, A., Lin, H., Aryal, D.K., McCorvy, J.D., Dengler, D., Corder, G., Levit, A., Kling, R.C., Bernat, V., Hübner, H., et al. (2016). Structure-based discovery of opioid analgesics with reduced side effects. Nature *537*, 185–190.

McCorvy, J.D., and Roth, B.L. (2015). Structure and function of serotonin G protein-coupled receptors. Pharmacol. Ther. *150*, 129–142.

McCoy, A.J., Grosse-Kunstleve, R.W., Adams, P.D., Winn, M.D., Storoni, L.C., and Read, R.J. (2007). Phaser crystallographic software. J. Appl. Cryst. *40*, 658–674.

Meltzer, H.Y., and Roth, B.L. (2013). Lorcaserin and pimavanserin: emerging selectivity of serotonin receptor subtype-targeted drugs. J. Clin. Invest. *123*, 4986–4991.

Moukhametzianov, R., Warne, T., Edwards, P.C., Serrano-Vega, M.J., Leslie, A.G., Tate, C.G., and Schertler, G.F. (2011). Two distinct conformations of helix 6 observed in antagonist-bound structures of a beta1-adrenergic receptor. Proc. Natl. Acad. Sci. USA *108*, 8228–8232.

Nichols, D.E. (2016). Psychedelics. Pharmacol. Rev. *68*, 264–355.

Palacios, J.M., Pazos, A., and Hoyer, D. (2017). A short history of the 5-HT2C receptor: from the choroid plexus to depression, obesity and addiction treatment. Psychopharmacology (Berl.) *234*, 1395–1418.

Pogorelov, V.M., Rodriguiz, R.M., Cheng, J., Huang, M., Schmerberg, C.M., Meltzer, H.Y., Roth, B.L., Kozikowski, A.P., and Wetsel, W.C. (2017). 5-HT2C Agonists Modulate Schizophrenia-Like Behaviors in Mice. Neuropsychopharmacology *42*, 2163–2177.

Preininger, A.M., Meiler, J., and Hamm, H.E. (2013). Conformational flexibility and structural dynamics in GPCR-mediated G protein activation: a perspective. J. Mol. Biol. *425*, 2288–2298.

Rasmussen, S.G., DeVree, B.T., Zou, Y., Kruse, A.C., Chung, K.Y., Kobilka, T.S., Thian, F.S., Chae, P.S., Pardon, E., Calinski, D., et al. (2011). Crystal structure of the β2 adrenergic receptor-Gs protein complex. Nature *477*, 549–555.

Roth, B.L. (2007). Drugs and valvular heart disease. N. Engl. J. Med. *356*, 6–9.

Roth, B.L., Sheffler, D.J., and Kroeze, W.K. (2004). Magic shotguns versus magic bullets: selectively non-selective drugs for mood disorders and schizophrenia. Nat. Rev. Drug Discov. *3*, 353–359.

Shapiro, D.A., Renock, S., Arrington, E., Chiodo, L.A., Liu, L.X., Sibley, D.R., Roth, B.L., and Mailman, R. (2003). Aripiprazole, a novel atypical antipsychotic drug with a unique and robust pharmacology. Neuropsychopharmacology *28*, 1400–1411.

Smart, O.S., Womack, T.O., Flensburg, C., Keller, P., Paciorek, W., Sharff, A., Vonrhein, C., and Bricogne, G. (2012). Exploiting structure similarity in refinement: automated NCS and target-structure restraints in BUSTER. Acta Crystallogr. D Biol. Crystallogr. *68*, 368–380.

Thal, D.M., Sun, B., Feng, D., Nawaratne, V., Leach, K., Felder, C.C., Bures, M.G., Evans, D.A., Weis, W.I., Bachhawat, P., et al. (2016). Crystal structures of the M1 and M4 muscarinic acetylcholine receptors. Nature *531*, 335–340.

Thomas, D.R., Gittins, S.A., Collin, L.L., Middlemiss, D.N., Riley, G., Hagan, J., Gloger, I., Ellis, C.E., Forbes, I.T., and Brown, A.M. (1998). Functional characterisation of the human cloned 5-HT7 receptor (long form); antagonist profile of SB-258719. Br. J. Pharmacol. *124*, 1300–1306.

Thomsen, W.J., Grottick, A.J., Menzaghi, F., Reyes-Saldana, H., Espitia, S., Yuskin, D., Whelan, K., Martin, M., Morgan, M., Chen, W., et al. (2008). Lorcaserin, a novel selective human 5-hydroxytryptamine2C agonist: in vitro and in vivo pharmacological characterization. J. Pharmacol. Exp. Ther. *325*, 577–587.

Toll, L., Berzetei-Gurske, I.P., Polgar, W.E., Brandt, S.R., Adapa, I.D., Rodriguez, L., Schwartz, R.W., Haggart, D., O'Brien, A., White, A., et al. (1998). Standard binding and functional assays related to medications development division testing for potential cocaine and opiate narcotic treatment medications. NIDA Res. Monogr. *178*, 440–466.

Tuplin, E.W., and Holahan, M.R. (2017). Aripiprazole, a drug that displays partial agonism and functional selectivity. Curr. Neuropharmacol. *15*, 1192–1207.

Venkatakrishnan, A.J., Deupi, X., Lebon, G., Tate, C.G., Schertler, G.F., and Babu, M.M. (2013). Molecular signatures of G-protein-coupled receptors. Nature *494*, 185–194.

Wacker, D., Fenalti, G., Brown, M.A., Katritch, V., Abagyan, R., Cherezov, V., and Stevens, R.C. (2010). Conserved binding mode of human beta2 adrenergic receptor inverse agonists and antagonist revealed by X-ray crystallography. J. Am. Chem. Soc. *132*, 11443–11445.

Wacker, D., Wang, C., Katritch, V., Han, G.W., Huang, X.P., Vardy, E., McCorvy, J.D., Jiang, Y., Chu, M., Siu, F.Y., et al. (2013). Structural features for functional selectivity at serotonin receptors. Science *340*, 615–619.

Wacker, D., Stevens, R.C., and Roth, B.L. (2017a). How ligands illuminate GPCR molecular pharmacology. Cell *170*, 414–427.

Wacker, D., Wang, S., McCorvy, J.D., Betz, R.M., Venkatakrishnan, A.J., Levit, A., Lansu, K., Schools, Z.L., Che, T., Nichols, D.E., et al. (2017b). Crystal structure of an LSD-bound human serotonin receptor. Cell *168*, 377–389.e12.

Wang, C., Jiang, Y., Ma, J., Wu, H., Wacker, D., Katritch, V., Han, G.W., Liu, W., Huang, X.P., Vardy, E., et al. (2013). Structural basis for molecular recognition at serotonin receptors. Science *340*, 610–614.

Wang, S., Wacker, D., Levit, A., Che, T., Betz, R.M., McCorvy, J.D., Venkatakrishnan, A.J., Huang, X.P., Dror, R.O., Shoichet, B.K., and Roth, B.L. (2017). D4 dopamine receptor high-resolution structures enable the discovery of selective agonists. Science *358*, 381–386.

Yadav, P.N., Abbas, A.I., Farrell, M.S., Setola, V., Sciaky, N., Huang, X.-P., Kroeze, W.K., Crawford, L.K., Piel, D.A., Keiser, M.J., et al. (2011a). The presynaptic component of the serotonergic system is required for clozapine's efficacy. Neuropsychopharmacology *36*, 638–651.

Yadav, P.N., Kroeze, W.K., Farrell, M.S., and Roth, B.L. (2011b). Antagonist functional selectivity: 5-HT2A serotonin receptor antagonists differentially regulate 5-HT2A receptor protein level in vivo. J. Pharmacol. Exp. Ther. *339*, 99–105.

STAR★METHODS

KEY RESOURCES TABLE

REAGENT or RESOURCE	SOURCE	IDENTIFIER
Antibodies		
HA Epitope Tag Antibody, Alexa Fluor 488 conjugate (16B12)	Thermo Fisher Scientific	Cat#A-21287 RRID: AB_2535829
Chemicals, Peptides, and Recombinant Proteins		
EDTA-free complete protease inhibitor cocktail tablets	Roche	Cat#5056489001
Iodoacetamide	Sigma	Cat#I1149
n-dodecyl-beta-D-maltopyranoside (DDM)	Anatrace	Cat#D310
Cholesterol hemisucinate (CHS)	Sigma	Cat#C6512
N-[4-(7-diethylamino-4-methyl-3-coumarinyl)phenyl]maleimide (CPM)	Invitrogen	Cat#D10251
TALON IMAC resin	Clontech	Cat#635507
1-Oleoyl-rac-glycerol (monoolein)	Sigma	Cat#M7765
Cholesterol	Sigma	Cat#C8667
Ergotamine D-tartrate	Sigma	Cat#45510-1G-F
Ritanserin	Tocris	Cat#1955
BrightGlo	Promega	Cat#E2620
RNA binding yttrium silicate beads	PerkinElmer	Cat#RPNQ0013
[^{3}H] mesulergine	PerkinElmer	Cat#NET1148
[^{3}H]-myo-inositol	Perkin Elmer	Cat#NET114A005
Poly-L-lysine	Sigma	Cat#P2636
Tetracycline	Sigma	Cat#T7660
Polyethyleneimine (PEI) solution	Sigma	Cat#P3143
Penicillin/Streptomycin	Invitrogen	Cat#15140-122
Puromycin	Gemini Bio-Products	Cat#400-128P
Hygromycin B	KSE Scientific	Cat#98-923
Blasticydin	Invivogen	Cat#ant-bl-10p
Zeocin	Invitrogen	Cat#R25005
Serotonin creatine sulfate monohydrate	Sigma	Cat#H7752
Primestar	Takara/Fisher	Cat# R045A
DpnI	New England Biolabs	Cat#R0176L
inositol-free DMEM	Caisson Labs	Cat#DML13
DMEM	VWR	Cat#45000-306
Fetal Bovine Serum (FBS)	VWR	Cat#97068-085
Dialyzed FBS	Omega Scientific	Cat#FB-03
10xHBSS	Invitrogen	Cat#14065-056
Fatty acid free bovine serum albumin	Sigma Aldrich	Cat# A7030-10G
L-Ascorbic acid	Sigma Aldrich	Cat# A92902-25G
MicroScint0 (scintillation fluid)	PerkinElmer	Cat# 6013611
Mianserin hydrochloride	Tocris	Cat# 0997
Clozapine	Tocris	Cat# 0444
Polyfect	QIAGEN	Cat# 301107
PfuUltra II Fusion Hotstart	Stratagene	Cat# 600672
Fatty acid free bovine serum albumin	Sigma Aldrich	Cat# A7030-10G

(*Continued on next page*)

Continued		
REAGENT or RESOURCE	SOURCE	IDENTIFIER
Deposited Data		
5-HT_{2C}-ergotamine complex structure	This paper	PDB code: 6BQG
5-HT_{2C}-ritanserin complex structure	This paper	PDB code: 6BQH
Experimental Models: Cell Lines		
Spodoptera frugiperda (*Sf9*)	A gift from Dr. Beili Wu (SIMM, CAS)	N/A
HEK293T	ATCC	Cat#CRL-3216
HTLA	A gift from Dr. Richard Axel, Columbia University	N/A
Flp-In T-Rex 293 Cell Line	Invitrogen	Cat#R78007
tsA201 cells	A gift from Dr. Penelope S.V. Jones, University of California	N/A
Oligonucleotides		
Primers for site-direct mutagenesis	This paper, see Table S7	N/A
Recombinant DNA		
Human 5-HT_{2C} gene	GenScript	N/A
h5-HT_{2C}-pCDNA3.1	Origine	N/A
pFastbac1	A gift from Dr. Raymond C. Stevens, University of Southern California	N/A
Software and Algorithms		
Schrödinger Suite 2015-4	Schrödinger	https://www.schrodinger.com/
XDS	Kabsch, 2010	xds.mpimf-heidelberg.mpg.de
SCALA	Collaborative Computational Project, Number 4, 1994	www.ccp4.ac.uk/html/scala.html
Phaser	McCoy et al., 2007	www.phenix-online.org
Phenix	Adams et al., 2010	www.phenix-online.org
Buster	Smart et al., 2012	www.globalphasing.com/buster
COOT	Emsley et al., 2010	www2.mrc-lmb.cam.ac.uk/personal/pemsley/coot
Prism	GraphPad Software	N/A
Other		
384-well black plates	Greiner Bio-one GmbH	Cat#781091
384-well white plates	Greiner Bio-one GmbH	Cat#781098
96-well black plates	Greiner Bio-one GmbH	Cat#655090
Meltilex	Perkin Elmer	Cat#1450-441
Filtermat A	Perkin Elmer	Cat#1450-421
100kDa cutoff concentrators	Sartorius	Cat#VS0642
96-well glass sandwich plates for LCP crystallization	NOVA	Cat#NOA90020

CONTACT FOR REAGENT AND RESOURCE SHARING

Further information and requests for resources and reagents should be directed to and will be fulfilled by the Lead Contact, Zhi-Jie Liu (liuzhj@shanghaitech.edu.cn).

EXPERIMENTAL MODEL AND SUBJECT DETAILS

Cell Lines

Spodoptera frugiperda (Sf9) cells were used for 5-HT_{2C} expression and crystallization. *Sf9* cells were grown in ESF 921 medium (Expression systems) at 27°C and 125 rpm. Binding and functional experiments were performed with either Flp-In 293 T-Rex stable cell lines (HEK293-derived, female, Invitrogen), HEKT cells (ATCC), tsA201 cells (female, gift from Dr. Penelope S.V. Jones) or HTLA

cells (HEK293-derived, female, gift from Dr. Richard Axel) that express TEV fused-β-arrestin2 and tTA-driven luciferase reporter (Barnea et al., 2008). HEKT cells were cultured in DMEM containing 10% fetal bovine serum (FBS) and 0.5% Penicillin/Streptomycin. Flp-IN 293 T-Rex cells were also cultured in DMEM with 10% FBS and 0.5% Penicillin/Streptomycin but also contained selection antibiotics, 10 μg/mL Blasticidin (Invivogen) and 100 μg/mL Hygromycin B (KSE Scientific). HTLA cells were also cultured in DMEM with 10% FBS and 0.5% Penicillin/Streptomycin but also contained selection antibiotics, 5 μg/mL Puromycin (Gemini Bio-Products) and 100 μg/mL Hygromycin B (KSE Scientific). The tsA201 cells were grown and maintained in culture medium [Dulbecco's Modified Eagle Medium supplemented with 10% fetal bovine serum, penicillin (100 U/mL) and streptomycin (100 μg/mL), all from Invitrogen] in a humidified atmosphere at 37°C and 5% CO_2.

METHOD DETAILS

The INI isoform of 5-HT_{2C} was selected for crystallography, pharmacological and mutagenesis experiments.

Rational Design of Thermostabilizing Mutations

To increase the thermostability and homogeneity of the 5-HT_{2C}, point mutations were rationally designed using a recently developed tool for GPCR stabilization mutation predictions. The tool starts with the sequence and structural models of the target GPCR, and explicitly evaluates all possible point mutations using four synergistic scoring models. These scoring models were derived using: (i) knowledge about previously characterized stabilizing mutations transferable between GPCRs; (ii) variations in sequences between closely related GPCRs; (iii) machine-learning algorithm trained on all known mutations in GPCRs; and (iv) structure-based information for residue interactions. A 3D homology model of human 5-HT_{2C} was constructed and refined with ICM molecular modeling suite (Abagyan and Totrov, 1994) using the X-ray structure of 5-HT_{2B} (PDB: 4IB4) (Wacker et al., 2013) as a template. The best 40 candidate point mutations predicted by the tool were selected for experimental validation. The candidates were analyzed for improvement of the 5-HT_{2C} monodispersity as evidenced by analytical size exclusion chromatography (aSEC) traces and thermal stability as evidenced by increase in Tm in the CPM assay (Alexandrov et al., 2008). Eight mutations were found to improve monodispersity and thermostability by more than 2 degree, of which the mutation C360N$^{7.45}$ was included into the engineered 5-HT_{2C} construct.

Protein Engineering for Structure Determination

The sequence of the human 5-HT_{2C} gene was synthesized by GenScript. The modified thermostabilized apocytochrome b_{562}RIL (BRIL) as a fusion partner was inserted into the receptor's third intracellular loop (IL3) at L246 and M300 of the human 5-HT_{2C} gene, using overlapping PCR. The construct was further optimized by truncation of N-terminal residues 1-39 and C-terminal residues 393-458. The ΔN-5-HT_{2C}-BRIL-ΔC DNA was subcloned into a modified pFastBac1 vector for expression in *Spodoptera frugiperda* (*Sf9*) cells. The chimera sequence has a haemagglutinin (HA) signal sequence followed by a FLAG tag at the N terminus, a PreScission protease site and a 10 × His tag at the C terminus. One rationally designed point mutation, C360N$^{7.45}$ (Table S7), was engineered into the 5-HT_{2C} gene by standard QuickChange PCR.

Protein Expression

The Bac-to-Bac Baculovirus Expression System (Invitrogen) was used to generate high-titer recombinant baculovirus (> 10^9 viral particles per ml). Recombinant baculovirus was produced by transfecting recombinant bacmids (2.5-5 μg) into *Spodoptera frugiperda (Sf9)* cells (2.5 mL, density of 10^6 cells per mL) using 5 μL of X-tremeGENE HP DNA Transfection Reagent (Roche) and Transfection Medium (Expression Systems). After 4 d of shaking at 27°C, P0 viral stock (~10^9 virus particles per mL) was harvested as the supernatant of the cell suspension to produce high-titer viral stock. Viral titers were analyzed by flow cytometry on cells stained with gp64-PE antibody (Expression Systems). 5-HT_{2C} was expressed by infecting *Sf9* cells at a cell density of 2-3 × 10^6 cells per ml with P1 virus at MOI (multiplicity of infection) of 5. Cells were harvested by centrifugation of 48 hours post infection and stored at −80°C for future use.

Protein Purification

Thawed insect cell membranes were disrupted in a hypotonic buffer containing 10 mM $MgCl_2$, 20 mM KCl, 10 mM HEPES (pH 7.5) and EDTA-free complete protease inhibitor cocktail tablets (Roche). The isolated raw membranes were extensively washed by twice repeated centrifugation in the same hypotonic buffer. Subsequently, soluble and membrane associated proteins were removed in a high osmotic buffer containing 10 mM $MgCl_2$, 20 mM KCl, 1.0 M NaCl, 10 mM HEPES (pH 7.5) and EDTA-free complete protease inhibitor cocktail tablets (three times). Purified membranes were flash-frozen in liquid nitrogen and stored at −80°C for further use.

Purified membranes were thawed at room temperature and incubated in the presence of 50 μM ERG or RIT and protease inhibitor cocktail at 4°C for 2 h. The membranes were incubated with 1.0 mg/mL iodoacetamide (Sigma) for 30 min and were solubilized in the buffer containing 50 mM HEPES (pH 7.5), 1% (w/v) n-dodecyl-beta-D-maltopyranoside (DDM, Anatrace), 0.2% (w/v) cholesterol hemisuccinate (CHS, Sigma-Aldrich) and 150 mM NaCl, at 4°C for 2.5 h. The solubilized 5-HT_{2C} proteins in the supernatants were isolated by high-speed centrifugation (Beckman), and then incubated at 4°C overnight with TALON IMAC resin (Clontech), 800 mM NaCl and 20 mM imidazole as the final buffer concentration. The resin was washed with 10 column volumes of washing buffer I containing 50 mM HEPES (pH 7.5), 0.1% (w/v) DDM, 0.02% (w/v) CHS, 800 mM NaCl, 10% (v/v) glycerol, 20 mM imidazole

and 50 μM ERG or RIT, and 6 column volumes of washing buffer II containing 50 mM HEPES (pH 7.5), 0.02% (w/v) DDM, 0.004% (w/v) CHS, 500 mM NaCl, 10% (v/v) glycerol and 50 μM ERG or RIT without imidazole. The protein was eluted using 4 column volumes of elution buffer containing 50 mM HEPES (pH 7.5), 0.02% (w/v) DDM, 0.004% (w/v) CHS, 500 mM NaCl, 10% (v/v) glycerol, 250 mM imidazole and 50 μM ERG or RIT. The 5-HT_{2C} protein sample was concentrated to ~30 mg/mL using a 100 kDa cutoff concentrator (Sartorius) for crystallization trials. The protein yield and monodispersity were measured by aSEC.

Lipidic Cubic Phase Crystallization

The purified 5-HT_{2C} protein in complex with ERG or RIT was screened for crystallization in lipidic cubic phase (LCP) with mixed molten lipid (90% (w/v) monoolein and 10% (w/v) cholesterol) at a protein/lipid ratio of 2:3 (v/v) using a mechanical syringe mixer (Caffrey and Cherezov, 2009). LCP crystallization trials were set up using an NT8-LCP crystallization robot (Formulatrix). 96-well glass sandwich plates were incubated at 20°C in an automatic incubator/imager (RockImager 1000, Formulatrix) and imaged. Crystals were obtained in 0.1 M sodium citrate pH 6.0, 80-120mM $(NH_4)_2SO_4$, 25%–32% PEG400, and grew to full size around two weeks. The crystals were harvested using micromounts (MiTeGen) and flash-frozen in liquid nitrogen.

Data Collection and Structure Determination

X-ray diffraction data of 5-HT_{2C}-ERG and 5-HT_{2C}-RIT crystals were collected at beam line 41XU at SPring-8, Japan, using a Pilatus3 6M detector, GM/CA at APS of Argonne National Lab, and X06SA beamline at the Swiss Light Source of the Paul Scherrer Institute, using Eiger 6M detector (X-ray wavelength 1.0000 Å). The data collection strategy was designed based on rastering results as previously described (Cherezov et al., 2009). Diffraction images were indexed, integrated and scaled using XDS (Kabsch, 2010) and merged using SCALA (Collaborative Computational Project, Number 4, 1994). Initial phases were obtained by molecular replacement (MR) method with Phaser (McCoy et al., 2007) using the receptor and BRIL portions of 5-HT_{2B} (PDB: 4IB4) as independent search models. In contrast to the 5-HT_{2C}-ERG, only receptor portion was found in the 5-HT_{2C}-RIT structure and partial BRIL was modeled during the refinement. Refinement was carried out with Phenix (Adams et al., 2010) and Buster (Smart et al., 2012) alternately followed by manual examination and adjustments of the refined structures in the program COOT (Emsley et al., 2010) with both 2|Fo|-|Fc| and |Fo|-|Fc| maps. In the final refined 2|Fo|-|Fc| maps, most of the 7TM structure and BRIL are ordered in the 5-HT_{2C}-ERG structure while full receptor and around 50% of the fusion partner BRIL are modeled in the 5-HT_{2C}-RIT structure.

Protein Stability Assays

Protein homogeneity was tested by aSEC using a 1260 Infinity HPLC system (Agilent). Protein thermostability was measured by a microscale fluorescent thermal stability assay as previously detailed (Alexandrov et al., 2008). For thermostability assay, CPM (*N*-([4-(7-diethylamino-4-methyl-3-coumarinyl) phenyl] maleimide) dye was dissolved in DMSO at 4 mg/ml as stock solution and diluted 1:20 in buffer (25 mM HEPES, pH 7.5, 500 mM NaCl, 5% (v/v) glycerol, 0.01% (w/v) DDM, 0.002% (w/v) CHS) before use. 1 μL of diluted CPM dye was added to the same buffer with approximately 0.5–2 μg 5-HT_{2C} receptor protein in a final volume of 50 μL. The thermal denaturation assay was performed in a Rotorgene realtime PCR cycler (QIAGEN). The excitation wavelength was 365 nm and the emission wavelength was 460 nm. All assays were performed over a temperature range from 25°C to 95°C. The stability data were processed with GraphPad Prism 6.0.

ERG Binding Target Profiling

The class A GPCR ERG target profiling was performed using a manual site search in the GPCRdb (Isberg et al., 2016) searching all receptors of the class for specific amino acids in the positions determined to be important for ERG binding in our structure- and sequence-based analysis of the ERG binding site. Specifically, the requirements for amino acids were as follows: position 3.32 - short and negatively charged (SN), i.e., Asp; position 3.33 - intermediate length and hydrophobic (IH), i.e., Ala, Ile or Val; position 3.36 and 5.42 - small and unbranched (SU), i.e., Ala, Cys, Gly or Ser; position 3.37 and 5.46 - very small or small and polar (VSP), i.e., Ala, Gly, Ser or Thr; position 6.51 and 6.52 - hydrophobic and maximum size of Phe (HF), i.e., Ala, Ile, Leu, Met, Phe or Val; position 209^{EL2} (in 5-HT_{2C}) - hydrophobic and aliphatic (HA), i.e., Ala, Ile, Leu, Met or Val. The search for high affinity ERG targets required all nine positions to match the aforementioned search criteria, while the search for low affinity ERG targets required Asp in position 3.32 but allowed non-matching amino acids in two of the other eight positions.

ChEMBL Privileged Structure Search

All ligands with $K_i < 1$ μM on any class A GPCR was retrieved from the ChEMBL (Bento et al., 2014) database (release CHEMBL22, https://doi.org/10.6019/CHEMBL.database.22) and searched for compounds containing the 4-arylpiperidine using Instant JChem 17.3.27.0, 2017, ChemAxon. The privileged structure was defined as a piperadine/piperazine ring connected to any heavy atom by a single/double bond, which is again connected to a six-membered aromatic ring. As the protonation is required, the nitrogen most distal from the aromatic ring cannot be part of an amine, sulfoneamide or be connected to any aromatic moiety. Furthermore, due to limited space in the pocket accommodating the privileged structure, position 2 and 3 on the aromatic ring should be unsub-stituted; substituents in position 4 and 5 are limited to non-cyclic moieties of only two heavy atoms.

Generation of 5-HT_{2C} Mutant Constructs

Mutagenesis of 5-HT_{2C} Flp-In 293 T-Rex and Tango constructs was performed using the Quikchange II XL site-directed mutagenesis protocol, except using Primerstar Max (Takara/Fisher) as the DNA polymerase. After DpnI (New England Biolabs) digest of parental DNA and transformation, positive colonies containing the mutation were selected using carbenicillin agar plates (Teknova). DNA was prepped using Maxi prep kits (Origene), and sequenced using the Sanger method by Genewiz (South Plainfield, New Jersey, USA).

Membrane Preparation and Radioligand Binding

For membrane preparation, HEKT (ATCC) cells (approximately 6 × 10^6 cells/15-cm dish) were transfected with 15 μg DNA per 15 cm dish of 5-HT_{2C} wild-type or mutant DNA (Table S7) using the calcium phosphate DNA precipitation method (Jordan et al., 1996). After 48 h transfection in DMEM containing 10% dialyzed FBS, cells were lysed using hypotonic lysis buffer (1 mM HEPES, 2 mM EDTA, pH 7.4) for 10 min, resuspended and centrifuged at 30,000 × g. After decanting of lysis buffer, membranes were resuspended in binding buffer (50 mM Tris, 10 mM $MgCl_2$, 0.1 mM EDTA, pH 7.4) and centrifuged at 13,000 × g in pre-chilled 1.7 mL centrifuge tubes. Buffer was decanted and membrane pellets were stored at −80°C until use.

Radioligand binding assays utilized [^{3}H]-Mesulergine (Perkin Elmer; Specific Activity = 84.7 Ci/mmol) at concentrations ranging from 0.7-1.3 nM, unlabeled ligand competitor at concentrations ranging from 100 μM to 1 pM, and membranes resuspended in binding buffer (50 mM Tris, 10 mM $MgCl_2$, 0.1 mM EDTA, 0.1% BSA, 0.01% ascorbic acid, pH 7.4). Binding assays were incubated at 37°C for 4 h and assays were terminated by vacuum filtration using a 96-well Filtermate harvester onto 0.3% polyethyleneimine pre-soaked 96-well filter mats A (Perkin Elmer). Filters were washed three times using cold wash buffer (50 mM Tris, pH 7.4) and scintillation cocktail (Meltilex) was melted onto dried filters. Radioactivity displacement was measured using a Wallac Trilux Microbeta counter (Perkin Elmer). Counts per minute (CPM) were plotted as a function of unlabeled ligand concentration and the K_i was calculated using the One-site-Fit K_i using Graphpad Prism 5.0. Data were normalized to the top (100%, no competitor) and bottom (0%, 10 μM 5-HT) to represent percent displacement.

For radioligand binding assays at all other receptors, procedures were similar as described except for the radioligand used and membrane sources. For a list of these binding assays refer to detailed procedures at https://pdspdb.unc.edu/pdspWeb/ for the National Institute of Mental Health Psychoactive Drug Screening Program (NIMH PDSP) (Besnard et al., 2012).

Test for RIT Selectivity Mutations

The RIT selectivity 5-HT_{2C} mutants were generated using Quikchange II XL site-directed mutagenesis (Stratagene, San Diego, CA) and oligonucleotides (TAG Copenhagen, Copenhagen, Denmark) (Table S7). After *Dpn*I (New England Biolabs) digest of parental DNA and transformation, positive colonies containing the mutation were selected using ampicillin agar plates. DNA was prepped using a Maxi prep kit (QIAGEN, Hilden, Germany), and the integrity of and the absence of unwanted mutations in all cDNAs generated by PCR were verified by DNA sequencing (Eurofins MWG Operon, Ebersberg, Germany).

The tsA201 cells were grown and maintained in culture medium [Dulbecco's Modified Eagle Medium supplemented with 10% fetal bovine serum, penicillin (100 U/mL) and streptomycin (100 μg/mL), all from Invitrogen] in a humidified atmosphere at 37°C and 5% CO_2. The cells were transiently transfected with wild-type and mutant h5-HT_{2C}-pcDNA3.1 constructs using PolyFect® (QIAGEN) according to the manufacturer's instructions. The culture medium was changed 16-20 h after transfection and membranes were harvested 36-48 h after transfection. The cells were scraped into harvest buffer (50 mM Tris-HCl, pH adjusted to 7.4 with NaOH), homogenized using an Ultra-Turrax for 10 s and centrifuged for 20 min at 50,000 × g. The resulting pellets were resuspended in fresh harvest buffer, homogenized and centrifuged at 50,000 × g for another 20 min, after which the pellet was stored at −80°C until use.

In the saturation binding experiments, the membranes were incubated with various concentrations (nine ranging from 0.03 nM to 10 nM) of [^{3}H]-mesulergine (Perkin-Elmer) in the absence (total binding) or the presence of 30 μM mianserin (non-specific binding) and, in competition binding experiments, the membranes were incubated with a fixed [^{3}H]-mesulergine concentration (0.5 nM or 2 nM, depending on the K_d value displayed by [^{3}H]-mesulergine at the specific receptor) and various concentrations of the test compounds (all from Tocris Cookson) in assay buffer (50 mM Tris-HCl, 10 mM $MgCl_2$, 0.1 M EDTA, 0.1% fatty acid-free bovine serum albumin and 0.01% ascorbic acid, pH adjusted to 7.4 with NaOH, freshly prepared each day) in a total volume of 300 μL. The experiments were performed in duplicate and the amount of membranes used was adjusted so that the bound/free ratios of [^{3}H]-mesulergine were ~10% or lower in all reactions. The mixtures were incubated for 2 h at 37°C and harvested into UniFilter 96-well GF/C plates using a FilterMate Harvester (PerkinElmer), washed with 2 mL/well wash buffer (10 mM Tris-HCl, 0.9% w/v NaCl, pH 7.4) and dried for at least 1 h at 50°C. 30 μL MicroScint0 (PerkinElmer) was added to each well in the filter, the plates were incubated for 1 h at room temperature, and the bound radioactivity were determined on a TopCount NXT scintillation counter. All data analysis was performed in GraphPad Prism 7.0b (GraphPad Software).

Phosphoinositide Hydrolysis (PI) Assay

Stable cell lines were generated in Flp-In 293 T-Rex cells expressing either 5-HT_{2C} wild-type or indicated mutants (Table S7). Phosphoinositide hydrolysis (PI) assays were performed using the scintillation proximity assay previously described (Bourdon et al., 2006; Huang et al., 2009). Briefly, tetracycline-induced cells (50-75,000 cells/well) were plated in inositol and serum-free DMEM (Caisson Labs) containing 1μCi/well of [^{3}H]-myo-inositol (Perkin Elmer) onto 96-well white plates. After 16-20 h, media was decanted, cells were washed and wells were replaced with 200 μL of inositol and serum-free DMEM. Drugs were diluted in drug buffer (20 mM

HEPES, 1X HBSS, 0.1% BSA, 0.01% ascorbic acid, pH 7.4) and 50 μL (5x) was applied to cells in concentrations ranging from 100 μM to 1 pM. Plates were incubated for either 60-120 min at 37°C and 5% CO_2. Lithium chloride (15 mM final concentration) was added to cells 15 min before lysis for IP capture and cells were lysed with 50 mM formic acid. Next day, 10 μL of lysate was added to 75 μL of 0.2 mg/well of RNA binding yttrium silicate scintillation beads (Perkin Elmer) in 96-well flexible, clear microplates. Plates were shaken for 1 h and centrifuged at 500 × g briefly for 1 min before reading on a Wallac MicroBeta Trilux plate reader (Perkin Elmer) measuring counts per minute (CPM). Data were analyzed using log (agonist) versus response (CPM) using Graphpad Prism 5.0. Data were normalized to percent 5-HT response, which was present in every experiment.

Tango Arrestin Recruitment Assay

The 5-HT_{2C} arrestin recruitment assays were performed as previously described (Cheng et al., 2016; Kroeze et al., 2015). Briefly, HTLA cells expressing the TEV fused-β-arrestin2 were transfected with 15 μg 5-HT_{2C} wild-type or mutant DNA per 15-cm dish in 10% dialyzed FBS DMEM. Next day, cells were plated into white 384-well plates at a density of 15,000 cells per well in 40 μL of 1% dialyzed FBS DMEM. After 6 h cells were stimulated with drugs ranging in concentration from 100 μM to 1 pM diluted in drug buffer (20 mM HEPES, 1X HBSS, 0.1% BSA, 0.01% ascorbic acid, pH 7.4) at a 5 × concentration. After 20-22 h of incubation at 37°C and 5% CO_2 media was decanted and 20 μL of BriteGlo (Promega, after 1:20 dilution) was added per well. After 20 min, plates were read on a Wallac MicroBeta Trilux (Perkin Elmer) at 1 s per well. Luminescence counts per second (LCPS) were plotted as a function of drug concentration and analyzed using log (agonist) versus response (LCPS) using Graphpad Prism 5.0. Data were normalized to percent 5-HT response, which was present in every experiment.

GPCRome Screening

Agonist activity at human GPCRome was determined as outlined previously (Kroeze et al., 2015) with modifications as indicated below. Briefly, HTLA cells were plated in poly-lysine coated 384-well white clear bottom plates in DMEM supplemented with 10% FBS (10,000 cells in 40 μL per well). After overnight incubation, cells received additional 10 μL/well of fresh DMEM supplemented with 50% FBS and transfected with receptor DNA (15 ng/well) for 24 h. Medium was removed and replaced with 40 μL/well of DMEM supplemented with 1% dialyzed FBS followed by 10 μL/well drug solution at 5 × of a final concentration (1, 3, and 10 μM). Medium with 1% dialyzed FBS served as basal for each receptor. After overnight incubation (~18 h), medium and drug solutions were removed and 20 μL/well of BrightGlo reagents (Promega) were added. Luminescence (Relative Luminescence Unit, RLU) was read on a luminescence reader, SpectraMax L (Molecular Devices), after 20 min incubation at room temperature. The assay was designed in this way so that 40 receptors were tested in each 384-well plate; each receptor had 4 replicate wells with testing drug and 4 replicate wells with vehicle control. Dopamine receptor D_2 serves as an assay control-16 replicate wells with 0.1 μM Quinpirole and 16 replicate wells with vehicle control. An additional 32 wells served as background control. Basal counts ranged from 70 – 120000 and were arranged in assay plates to avoid/minimize cross-talk, as described previously (Kroeze et al., 2015). Each GPCRome screening needs a total of 8x 384-well plates. Results were presented in the form of fold over basal for each receptor and plotted in the GraphPad Prism.

Docking of Lorcaserin

All molecular modeling calculations mentioned in this section were performed using modules (Maestro, Ligprep, Protein Preparation Wizard and Glide) in the Small-Molecule Drug Discovery Suite 2017-2, Schrödinger, LLC, New York, NY, 2017. Lorcaserin was built in Maestro using the 2D-sketcher and the 3D-structure was generated using LigPrep with default settings. The 5-HT_{2C}-ERG structure was preprocessed and optimized with default settings in the Protein Preparation Wizard and a docking grid was calculated with Glide defining the binding site by selecting ERG and setting the ligand diameter midpoint box to 12 Å on all three axes – otherwise default settings. Finally, lorcaserin was docked into the calculated receptor grid using the XP scoring function, a scaling factor of 0.7 and partial charge cutoff of 0.2 to compensate for the lack of the forcefield to correctly take halogen bonds into account. Additionally, five output poses were specified, post-docking minimization was disabled. The best ranking of only two suggested similar binding modes were selected.

QUANTIFICATION AND STATISTICAL ANALYSES

Dose-Response and Binding Affinity Calculations

Dose-response data and radioligand displacement data were analyzed using Graphpad Prism 5.0. Dose-response data were fit using log (agonist) versus response function, which constrains the hill slope to 1. Estimates of E_{MAX} and EC_{50} were fit and data were normalized to a reference ligand (for 5-HT_{2C} reference was 5-HT) and averaged across independent experiments using Graphpad Prism 5.0. Specific [^{3}H]-mesulergine binding and K_d values of the radioligand at the various receptors were determined based on fitting of the saturation binding data to a one-site total and non-specific equation and K_i values were calculated based on the IC_{50} values extracted from concentration-inhibition curves derived from the competition binding data using the Cheng-Prusoff equation in Graphpad Prism 5.0.

Test for RIT Selectivity Mutations

For K_d and pK_i analysis, we have one dependent variable (K_d or pK_i), and the independent variable(s) consists of several categorical independent groups. For K_d we are comparing the [^{3}H]-mesulergine binding of each mutant against the WT receptor (one independent group). For pK_i, we are comparing each compound at each mutant against that compound at the WT receptor (two independent groups). Since K_i is determined from a logarithmic scale of compound concentration, all further calculations are done with pK_i values. Our data contained no significant outliers, as determined using the ROUT analysis from GraphPad Prism with the false discovery rate set to 1%. Our sample size is too small to meaningfully test for normal distribution, but all K_d and pK_i values do pass the Shapiro-Wilk normality test with $\alpha = 0.05$, and a normal distribution is assumed for all groups. The number of independent repeats is similar between groups and/or the variance is similar between groups. Not all mutants were tested on each assay day. We have thus elected to use a non-paired one-way ANOVA for the K_d comparison, and a non-paired two-way ANOVA for the pK_i comparison. Since we, in both K_d and pK_i comparisons, are comparing a control (WT) mean with other means, we have used the Dunnetts post-test for both to avoid the artifact of falsely wide confidence intervals often resulting from using Tukey's post-test for many-to-one comparisons.

DATA AND SOFTWARE AVAILABILITY

Data Resources

The accession numbers for the coordinates and structure factors of 5-HT_{2C}-ERG and 5-HT_{2C}-RIT are PDB: 6BQG and PDB: 6BQH, respectively.

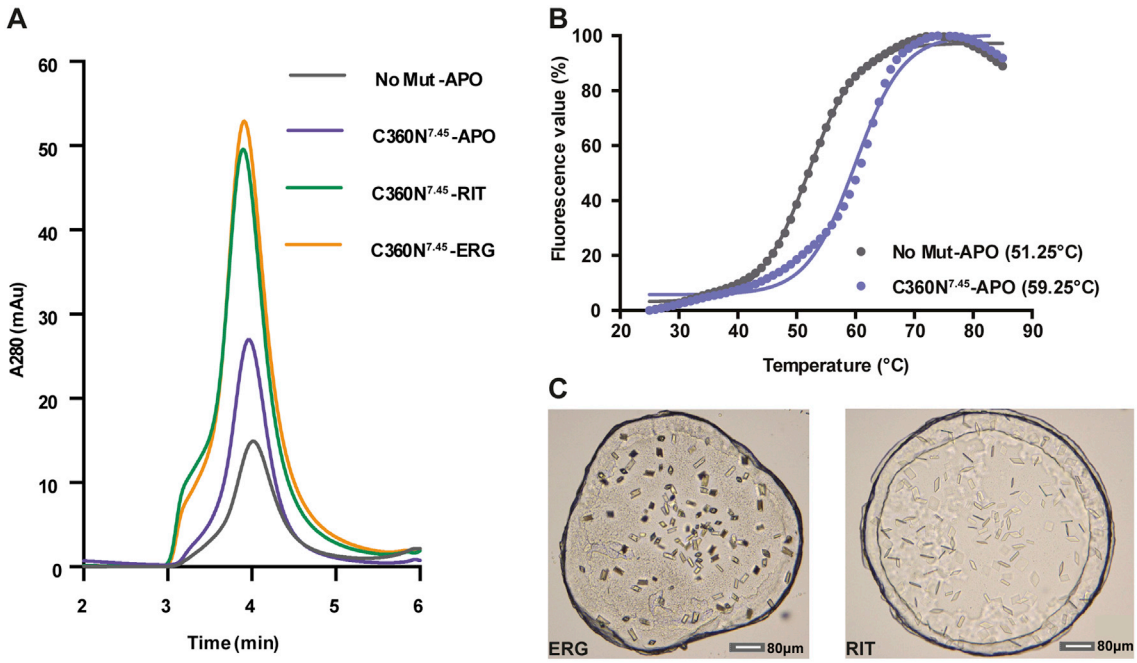

Figure S1. Stability Assay of 5-HT_{2C} Mutant, Ligands, and Crystal Images, Related to Figure 1

(A) Analytical size exclusion chromatography (aSEC). No Mut-APO: N/C-terminal truncated and BRIL inserted into the IL3 construct without mutation and without ligand (gray); $C360N^{7.45}$-APO: $C360N^{7.45}$ mutated in the engineered construct without ligand (purple); $C360N^{7.45}$-RIT: $C360N^{7.45}$-APO with RIT (green); $C360N^{7.45}$-ERG: $C360N^{7.45}$-APO with ERG (orange).

(B) CPM thermostability ramping assay of 5-HT_{2C} at different forms of protein as tested.

(C) Crystal images of 5-HT_{2C} bound to ERG and to RIT. The length of the reference white band is 80 μm.

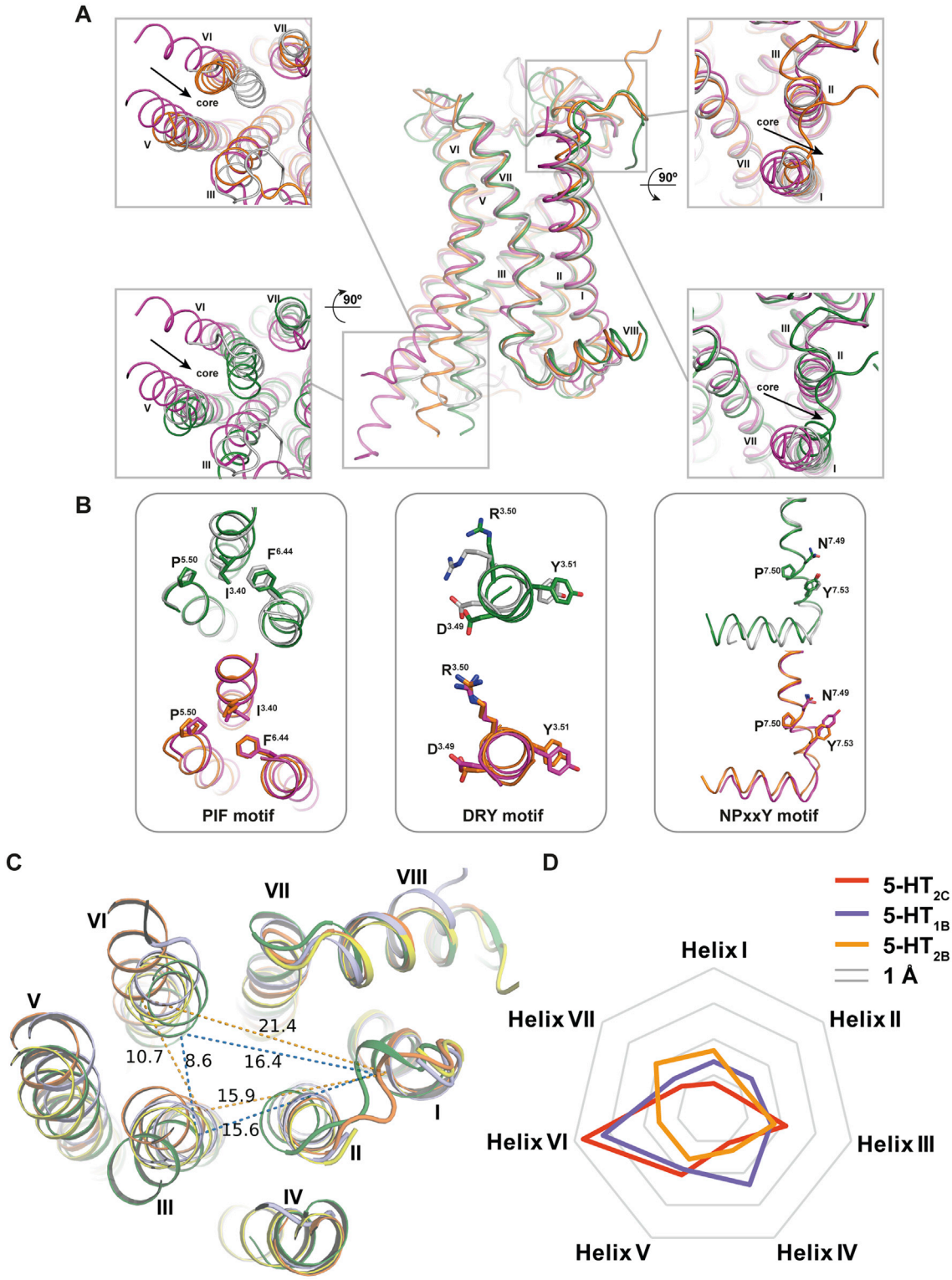

Figure S2. Structural Alignment of 5-HT$_{2C}$-ERG and 5-HT$_{2C}$-RIT with β_2AR in the Active State (PDB: 3SN6) and Inactive State (PDB: 3NY8) and Differences in the Relative Location at the Ends of Intracellular Helices in Four Serotonin Receptors Crystal Structures, Related to Figure 1

(A) 5-HT$_{2C}$-ERG, orange; 5-HT$_{2C}$-RIT, green; active state β_2AR, magenta; inactive state of β_2AR, gray. (Left panel) Intracellular view. (Right panel) Extracellular view.

(legend continued on next page)

(B) The conformation similarities of the trigger motifs PIF, DRY, and NPxxY in 5-HT_{2C}-ERG versus active state β_2AR and 5-HT_{2C}-RIT versus inactive state of β_2AR structures, respectively.

(C) Four crystal structures (5-HT_{2C}-RIT: green, 5-HT_{2C}-ERG: orange, 5-HT_{1B}-ERG: light blue (PDB: 4IAR) and 5-HT_{2B}-ERG: yellow (PDB: 4IB4)) represented as cartoons and viewed from the intracellular side. Representative distances between C_α atoms of $V78^{1.57}$, $I148^{3.46}$ and $L313^{6.37}$ (selected to be at the same helical height) are shown as dashed lines with labeled distances in Å. The 5-HT_{2C} structures with ERG and RIT show the largest and smallest inter-helical distances in the intracellular ends, respectively.

(D) A schematic illustrating the differences in relative positions of the TM helices defined by RMSDs between ERG-bound 5-$HT_{1B,2B,2C}$ and RIT-bound 5-HT_{2C} structural conformations.

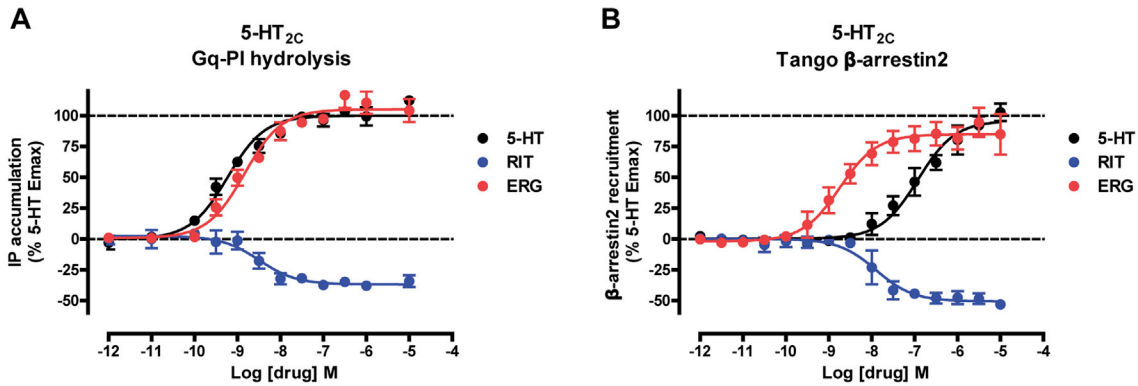

Figure S3. Pharmacological Profile of ERG and RIT at 5-HT$_{2C}$, Related to Figure 3

(A and B) ERG shows potent agonism and RIT shows inverse agonist activity for both (A) $G_{\alpha q}$-dependent and (B) $G_{\alpha q}$-independent β-arrestin2 recruitment to the 5-HT$_{2C}$. Data represent mean ± SEM from at least four independent experiments performed in triplicate.

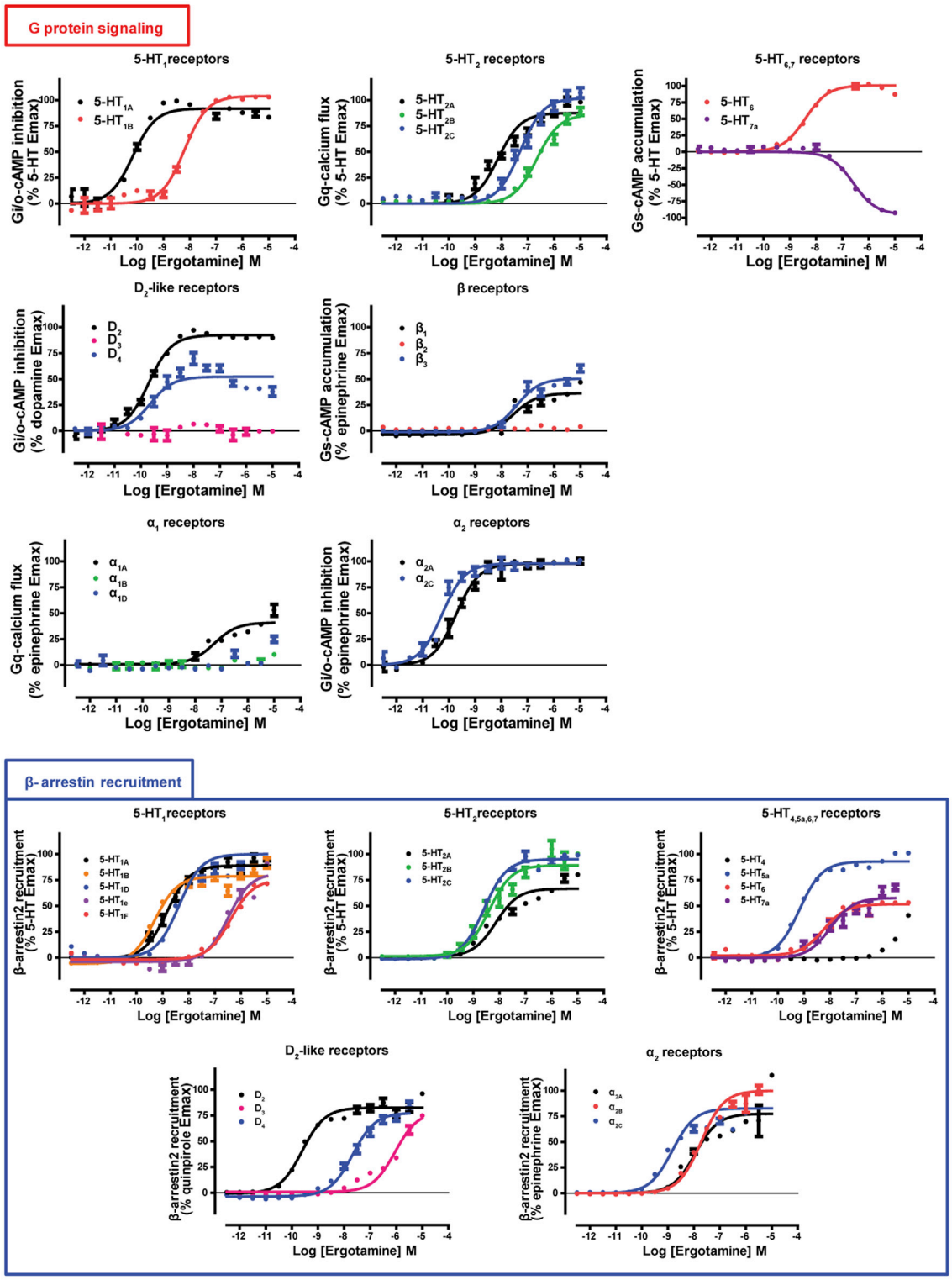

Figure S4. Analysis of the Function of ERG on a Panel of Aminergic Receptors, Related to Figure 4

Analysis of the function of ERG on a panel of aminergic receptors shows the varied profile of ERG as agonist, inverse agonist, or antagonist at select receptors. The functional profile includes either G protein-dependent activity and β-arrestin2 recruitment or both for adrenergic, dopamine, and serotonin receptors. All receptors tested are human wild-type aminergic receptors. Data performed in triplicate and represent mean ± SEM from at least three independent experiments.

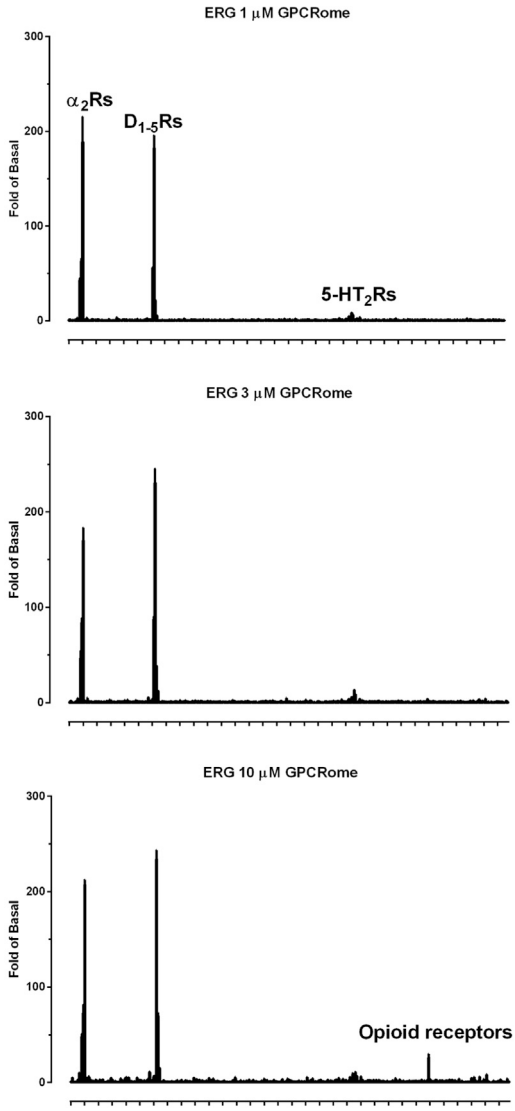

Figure S5. GPCRome Screening Results, Related to Figure 4

Screening of ERG across the GPCRome (at 320 receptors) using the PRESTO-Tango platform with ergotamine present at 1μM, 3 μM, and 10 μM concentrations. Additional details on method, basal activities, and plate arrangement can be found in the methods.

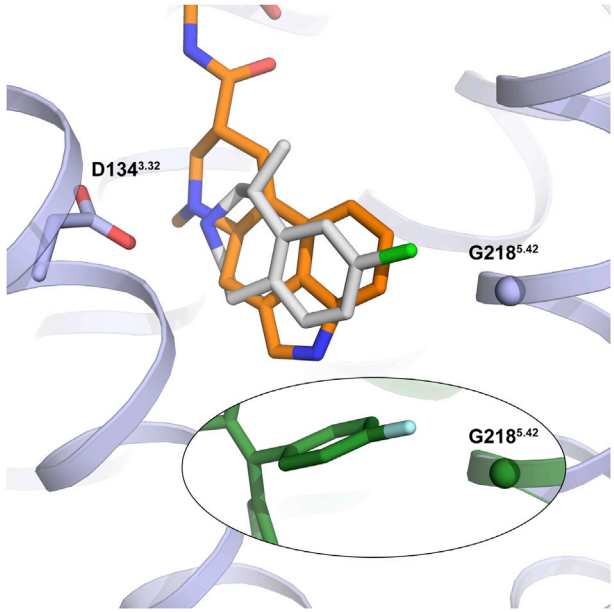

Figure S6. Binding Mode and Mechanism of Selectivity for Lorcaserin, Related to Figure 6

Docking binding mode of lorcaserin (white sticks) in the 5-HT2C-ERG structure (light blue cartoon and orange sticks) showing similar location of the protonated amines and aromatic moieties. In addition, the binding pose of lorcaserin is comparable to RIT in the 5-HT_{2C}-RIT structure (green cartoon and sticks in the inset), the chlorine of lorcaserin is in close proximity to the Cα atom of the 5-HT_2 group-unique residue, G218$^{5.42}$, and can explain the reported binding selectivity of lorcaserin for these receptor subtypes (Thomsen et al., 2008). The figure was prepared using The PyMOL Molecular Graphics System, Version 1.8 Schrödinger, LLC.